View metadata, citation and similar papers at core.ac.uk

brought to you by CORE

provided by ScholarBank@NUS

Realistic Simulation of Forward and Reverse Characteristics of 4H-SiC pn Junction Diode

WEI GUANNAN

NATIONAL UNIVERSITY OF SINGAPORE

2008

Realistic Simulation of Forward and Reverse Characteristics of 4H-SiC pn Junction Diode

Wei Guannan

A THESIS SUBMITTED

FOR THE DEGREE OF MASTER OF ENGINEERING

DEPARTMENT OF ELECTRICAL AND COMPUTER ENGINEERING

NATIONAL UNIVERSITY OF SINGAPORE

2008

ACKNOWLEDGEMENT

In the first place I would like to express my earnest gratitude to Professor Yung C. Liang and Professor Ganesh S. Samudra for their supervision, advice, and guidance all along this research. Their in-depth intuition have exceptionally inspired and enriched my growth as a student, which will greatly benefit my future. During my hard times, they provided me a constant spring of ideas, unflinching encouragement and warm support. I am very grateful for their precious time, invaluable suggestions and constructive comments in my research and also this thesis.

Secondly my parents, Wei Li and Cao Aimin, deserve special mention for their inseparable support and care. They raised me with their endless love, built my learning character from childhood and enlightened my interest in intellectual pursuit. Their dedication, patience and persistent confidence in me have taken the load off my shoulder.

Collective and individual acknowledgements are also owed to my friends in Power Electronics Lab, for creating a pleasant and colorful research environment. Many thanks go in particular to my senior Chen Yu for her generous technical help, plentiful discussions and unselfishly sharing the bright thoughts.

Finally, I would like to thank everybody who was important to the successful realization of this thesis, as well as expressing my apology that I could not mention all the names that have helped me during my time in National University of Singapore.

Name: Wei Guannan
Degree: Master of Engineering
Department: Electrical and Computer Engineering (ECE)
Title: Realistic Simulation of Forward and Reverse Characteristics of 4H-SiC pn Junction Diode

ABSTRACT

This thesis presents a methodology to simulate the forward and reverse characteristics of realistic 4H-SiC pn junctions. The superior property of SiC and motivation of this work are explained. The simulation models and parameters for forward and reverse characteristics of realistic 4H-SiC pn junctions are reviewed. The physical bases behind methodology of the simulation improvement are discussed. The extensive collection of reported 4H-SiC pn junction diode data formed the basis of calibration of SYNOPSYS MEDICI for 4H-SiC pn junction simulation. Relevant parameters in the trap and photogeneration models are modified for realistic simulations. Motivation and justification of the modifications are presented. A universally applicable model parameter set for simulation of the forward and reverse characteristics of practical 4H-SiC pn junction is proposed and verified against reported independent data not used in the calibration step.

Keywords: Simulation, MEDICI, 4H-SiC pn junction diode, defects, dislocation, Trap, Photogeneration

CONTENTS

Acknowledgement

List of Figures

List of Symbols

List of Tables

Summary

Chapter 1. Introduction ....- 1-

1.1. Benefits of SiC Material in Power Devices ....- 1-

1.1.1. High power application ....- 1-

1.1.2. High frequency application ....- 2-

1.1.3. High temperature application ....- 3-

1.2. Introduction to SiC polytypes ....- 4-

1.3. SiC power devices ....- 6-

1.4. Motivation for simulation improvements ....- 7-

1.5. Thesis outline ....- 9-

Chapter 2. Current process technology ....-11-

2.1. SiC bulk growth technology ....- 11-

2.1.1. History of Bulk growth of SiC wafers ....- 11-

2.1.2. Seeded sublimation growth technology ....- 13-

2.1.3. Commercial SiC wafers ....- 14-

2.1.4. Bulk crystal defects ....- 15-

2.2. SiC epitaxial growth technology ....- 17-

2.2.1. General Epitaxial growth technology of SiC ....- 17-

2.2.2. High temperature CVD (HTCVD) ....- 18-

2.2.3. Epilayer crystal defects ....- 19-

2.3. Ion implantation and annealing in SiC ....- 21-

2.3.1 Ion implantation in SiC - 21-

2.3.2. Defects induced by Ion implantation - 22-

2.3.3. Annealing - 23-

2.3.4. Defects induced by annealing - 23-

2.4. Summary - 25-

Chapter 3 - 26 -

Models and Parameters for 4H-SiC Electrostatic Simulation - 26 -

3.1. Introduction of MEDICI - 26 -

3.2. Intrinsic Carrier Concentration and Energy Bandgap - 30 -

3.3. Carrier Mobility - 33 -

3.3.1. Low field mobility - 33 -

3.3.2. High field mobility - 35 -

3.3.3. Anisotropy in Mobility - 37 -

3.4. Generation and Recombination - 39 -

3.4.1. Shockley-Read-Hall Recombination - 39 -

3.4.2. Auger Recombination - 41 -

3.4.3. Impact ionization - 41 -

3.4.4. photogeneration - 44 -

3.5. Trap Model - 46 -

3.6. Summary - 49 -

Chapter 4 - 50 -

Realistic Simulation of Reverse Characteristics of 4H-SiC pn Junction Diode - 50 -

4.1. Reverse blocking ability and impact ionization in 4H-SiC pn junction - 50 -

4.1.1. Basic equations - 51 -

4.1.2. Multiplication coefficient M and breakdown criteria - 53 -

4.1.3. Breakdown voltages and critical fields in 4H-SiC - 55 -

4.2. Challenge and consideration in simulation of reverse characteristics of SiC pn junction in MEDICI - 60 -

4.3. Simulation methodology of breakdown voltage of 4H-SiC pn junction diode .....- 61 -
4.3.1. Physical analysis ....- 61 -
4.3.2. Simulation methodology ....- 66 -
4.4. Simulation methodology of reverse current in 4H-SiC pn junction diode ....- 72 -
4.4.1. Physical analysis ....- 72 -
4.4.2. Simulation methodology ....- 72 -
4.4.3. Simulation result and verification ....- 75 -
4.5. Summary........- 78 -

Chapter 5 ....- 79 -
Realistic Simulation of Forward Characteristics of 4H-SiC pn Junction Diode ....- 79 -
5.1. Forward characteristics of 4H-SiC pn junction ....- 79 -
5.1.1. Recombination without injection ....- 79 -
5.1.2. Low level injection ....- 80 -
5.1.3. High level injection ....- 84 -
5.2. Realistic simulation of forward characteristics of 4H-SiC pn junction diode ....- 85 -
5.2.1. Simulation considerations ....- 85 -
5.2.2. Simulation models and physical parameter values ....- 85 -
5.2.3. Simulation result and discussion ....- 88 -
5.3. Summary........- 92 -

Chapter 6. Conclusion........- 93 -

Reference........- 96 -

LIST OF FIGURES

	Figure Caption	Page
Figure 1-1:	The crystal structure of 3C-, 2H-, 4H- and 6H-SiC	4
Figure 1-2:	Summary of the Silicon Carbide electronic devices.	6
Figure 1-3:	Comparison of reported experimental result and simulation result of reverse characteristics of 4H-SiC pn diode. The large mismatch shows that the simulation of practical SiC device needs improving.	10
Figure 2-1:	Cross section of a crucible in Lely process for crystal growth	13
Figure 2-2:	Cross section of crucibles for modified Lely and typical temperature profile (a).Lid mounting of the seed. (b) Bottom mounting of the seed	14
Figure 2-3:	Principal axes for hexagonal crystal	15
Figure 2-4:	Possible defects. a) Inclusion giving rise to a hollow core; b) Screw dislocation c) Inclusion giving rise to two screw dislocations of opposite sign.	16
Figure 2-5:	CVD setup for epitaxial growth of SiC	18
Figure 3-1:	Intrinsic carrier concentration for 4H SiC and Si VS Temperature.	32
Figure 3-2:	Drift velocity of electron in 4H SiC as functions of the applied field.	37
Figure 4-1:	Electric field for normal p-i-n diode under reverse bias	51
Figure 4-2:	Hole impact ionization coefficients for 4H-SiC	56
Figure 4-3:	Two forms of hole impact ionization coefficients for 4H-SiC at 300K	57
Figure 4-4:	Hole and electron impact ionization coefficients for 4H-SiC at 300K	59
Figure 4-5:	Impact ionization coefficients and their poly form for 4H-SiC at 300K	59
Figure 4-6:	Breakdown field VS doping concentration in 4H-SiC	60

Figure 4-7:	The schematic diagram of some common SiC epilayer defects	62
Figure 4-8:	Spiral ramp of a screw dislocation with Burger vector *b*	64
Figure 4-9:	Model of ideal screw dislocation.	64
Figure 4-10:	Breakdown voltage of 4H-SiC pn junction diodes vs. Trap density applied in TRAP model	69
Figure 4-11:	Breakdown voltage of 4H-SiC pn junction diodes vs. Trap density applied in TRAP model.	70
Figure 4-12	Influence of A1 to reverse current	75
Figure 4-13:	Experimental and simulated reverse current characteristics of 4H-SiC pn junction diodes.	76
Figure 4-14:	Experimental and simulated reverse current characteristics of 4H-SiC pn diodes junction.	76
Figure 4-15:	Application of the methodology to predict reversed current characteristics of a reported 4H-SiC pn junction diode.	77
Figure 5-1:	A scheme of a pn junction diode under low injection condition	81
Figure 5-2:	Different slop of forward characteristics caused by high level injection	84
Figure 5-3:	a) Reported forward characteristics[5.4], b) Simulation result	88
Figure 5-4:	a) Reported forward characteristics[5.5], b) Simulation result	88
Figure 5-5:	Result of forward characteristics simulation with defects of 4H-SiC pn junction diode reported in [5.4]	89
Figure 5-6:	Result of forward characteristics simulation with defects of 4H-SiC pn junction diode reported in [5.5]	89
Figure 5-7:	Influence of bandgap energy to the forward current reported in [5.5]	90
Figure 5-8:	Influence of lifetime to the forward current reported in [5.5]	91
Figure 5-9:	Influence of hole mobility to the forward current reported in [5.5]	91

LIST OF SYMBOLS

A_1	Injected carrier concentration	N_A^-	Ionized accepter concentrations
α_n	Electron ionization coefficient	N_D^+	Ionized donor concentrations
α_p	Hole ionization coefficient	N_{t_i}	Total number of traps at level i
D_n	Hole diffusivity	N.TOTAL	Trap density in MEDICI
D_p	Electron diffusivity	p	Hole concentration
D_{trap}	Trap density	ρ_s	Surface charge density
E	Electric field	q	Electron charge
E_c	Critical electric field	T	Temperature
E_g	Bandgap energy	U_n	Electron recombination rate
E_{max}	Maximum electric field	U_p	Hole recombination rate
E_{t_i}	Trap level energy for level i	μ_n	Electron mobility
ε	Dielectric permittivity	μ_p	Hole mobility
ε_{SiC}	Permittivity of SiC	V_{BD}	Breakdown voltage
G	Generation rates	W	Width of drift region
J	Current density	W_D	Width of depletion region
M	Multiplication factors	ψ	Intrinsic Fermi potential
n	Electron concentration	ϕ	Quasi-Fermi level
n_i	Intrinsic doping concentration	τ_n	Electron lifetime
N	Drift region doping concentration	τ_p	Hole lifetimes

LIST OF TABLES

	Table Caption	Page
Table 1-1:	Material properties of Si, 3C-SiC, 6H-SiC, and 4H-SiC at 300 K	5
Table 1-2:	Best reported high voltage SiC devices	7
Table 3-1:	Parameters of low field mobility for 4H-SiC at 300K.	35
Table 3-2:	Parameters of high field mobility for 4H-SiC at 300K and 593K	37
Table 3-3:	Parameters of impact ionization model for 4H-SiC	44
Table 4-1:	Reported data of 4H-SiC pn junction diodes and simulation result with adjusted trap density	70
Table 4-2:	Verification for simulation result	71

Summary

The superior material properties of SiC such as high electric field strength, high saturation drift velocity, and high thermal conductivity make SiC a very promising wide band material in high power, high temperature and high frequency application area. The unique feature of SiC, polytypism, is specially described and the motivation to choose the polytype 4H-SiC for this work is explained. As the technology and research study in SiC devices are progressing rapidly, a good simulation methodology to predict performance of these devices will be very useful for the industry and researchers. A reasonably accurate and predictive methodology to simulate the forward and reverse characteristics of 4H-SiC pn junction diodes with varying doping concentration and junction depth has been developed and presented in this thesis.

One main reason leading to the large mismatches of simulation results with reported device characteristics is the immaturity of the fabrication process and the defects induced by these processing techniques. The main process techniques for SiC pn junction diode, such as bulk and epitaxial growth, ion implantation and annealing process, and the defects caused are studied. Based on the study of the defects induced by each process, the main defect affecting the SiC device performance is analyzed to be elementary screw dislocation, which should be taken into consideration in simulation of SiC device.

There are two models should be specially incorporated in simulation of reverse state

practical 4H-SiC pn junction diode, photogeneration and trap model. Photogeneration can be applied to increase to carrier concentration at the pn junction at the beginning of the simulation. Parameter A1 can be used to adjust simulation current depending on 4H-SiC doping concentration, substrate quality and fabrication environment. Another model is TRAP model, which can take the influence of dislocations to the simulation into account. The trap energy and density can be specified in the trap model. A collection of data of reported 4H-SiC pn junction diodes of typical design are studied. An expression of trap density as a function of drift layer thickness and doping concentration is obtained, which is verified by applying the calculated trap densities to other reported 4H-SiC pn junction diodes.

Models and parameters with physical values for simulation of forward conduction characteristics of 4H-SiC pn junction diode are summarized. Two reported 4H-SiC pn junction diodes are simulated by specifying the physical material parameters values. The result shows that the forward characteristics of realistic 4H-SiC pn junction diodes can be simulated in MEDICI by specified the parameters with material physical value and without incorporating TRAP model.

At the end of thesis, it is considered that the physical mechanism of creating the defects during fabrication process has not been studied in depth. Further study could be done on this topic and incorporate this mechanisms into the simulation for its further improvements.

Chapter 1

Introduction

Silicon carbide is a wide energy bandgap semiconductor material, which possesses a combination of material and electrical parameters that make it advantageous for various applications in the semiconductor industry. This introductory chapter will present the material advantages of SiC and general review of current SiC devices. The motivation of the work and the outline of this thesis will be presented as well.

1.1. Benefits of SiC Material in Power Devices

SiC has many superior physical properties such as high breakdown electric field, high saturation drift velocity, and high thermal conductivity. These have made SiC a very promising wide band material in high power, high temperature and high frequency application area. Compared with other wide energy bandgap semiconductors, SiC has great advantages because of rapidly maturing technology for single crystal substrates [1.1] and the ability to form thermal SiO_2 on Si in a similar way with Si.

1.1.1. High power application

For power-device applications, the most important property of a semiconductor material is the breakdown electric field strength. This property determines how high the largest field in the material may be before material bulk breakdown takes place. Because of the wide bandgap, the impact ionization energy is very high in SiC. This means that SiC can

sustain very high field before onset of impact ionization. In Si, the critical electric field is 0.25 MeV/cm [1.2]. For SiC, the critical electric field can be ten times higher than Si. Hence the devices fabricated using SiC can have ten times higher breakdown voltage than similar devices using Si that have the same drift region width. The exact breakdown electric field marginally depends on the doping concentration and increases with increasing doping in Si.

The second most important parameter besides critical electric field for power device application is thermal conductivity of the material on which the devices are fabricated. An increase in temperature usually leads to a change in the physical properties of the device, which normally affects the device performance negatively. For example, the carrier mobility decreases with increasing temperature reducing the device current. Therefore, the heat generated through various resistive losses during operation must be conducted away from the hot-spots in the device area to the package. The high thermal conductivity of SiC allows high power density. The thermal conductivity of SiC is three time higher than Si, which allows three times higher thermal flow to be accommodated under the same temperature increase at the junction. Amazingly, the thermal conductivity of SiC is higher than that of copper at room temperature and most of the metals at room temperature [1.2].

1.1.2. High frequency application

From the description of section 1.1.1 to 1.1.3, the critical features for devices in SiC can be made much smaller than those in Si for the same breakdown voltage. Therefore, the device is faster, since the signal has a shorter distance to travel and reduction in features

will also reduce various parasitic capacitances. The relative dielectric constant is also lower for SiC than for most other semiconductor, which means that parasitic capacitances will even be further reduced. However, for high frequency devices, the breakdown electric field strength is not as important as the saturated drift velocity. The saturated electron velocity in SiC is as twice as that of Si and GaAs. A high saturated drift velocity is advantageous in order to obtain high channel currents for microwave devices. Semi-insulating single crystal substrates are available in SiC like in GaAs which can contain substrate losses in microwave applications.

1.1.3. High temperature application

In semiconductor, the bandgap energy is the minimum energy which is needed to excite an electron from the valence band to the conduction band. Thermal energy through lattice vibrations can create electron-hole pairs in the semiconductor even at room temperature. If the temperature is high enough, thermally generated electron-hole pairs can exceed the number of free carriers from the impurity doping. When this occurs, the material becomes intrinsic and the devices fail, as there is no longer any p-n junction to block the voltages because of the free carrier concentration increase. The threshold for this to occur is the intrinsic temperature, where thermal generation is too high. Thus, the intrinsic temperature depends on dopings. For high temperature devices, higher doping may be used to raise the intrinsic temperature. Because of wide bandgap, SiC has a high intrinsic temperature around 1000℃, which depends on polytype and doping. The SiC devices will normally not reach such a high temperature as other failures, such as contact failure, which will happen at much lower temperature.

1.3. SiC polytypes

SiC has a unique feature, polytypism [1.3]. The polytypes are named according to the periodicity of these layers and the overall symmetry of the crystal structure. Each bonded Si-C bilayer can be situated in one of three possible positions with respect to the lattice. These possible positions can be assigned by A, B, or C notation as shown in Figure 1-1. Depending on the stacking order, the bonding between Si and C atoms in adjacent bilayer planes has either a cubic or hexagonal symmetry. For example, one popular polytype subject to extensive study is 4H-SiC, which is a hexagonal type lattice and has four Si + C layers in one periodicity which will repeat afterwards, ABAC, ABAC,ABAC……. The crystal structure of 3C-, 2H-, 4H- and 6H-SiC is also shown in Figure 1.

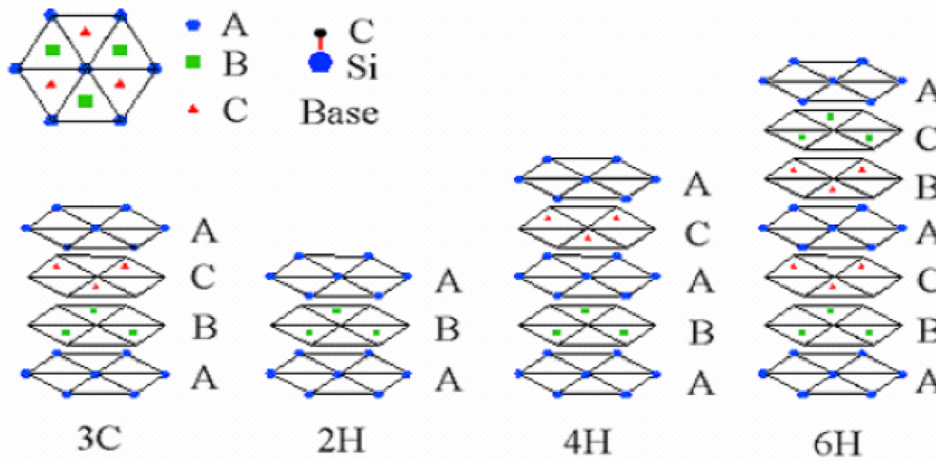

Figure 1-1. The crystal structure of 3C-, 2H-, 4H- and 6H-SiC

Of the numerous polytypes of SiC, initial work focused on 3C polytype due to the superior transport properties. However, the technology for growing 3C-SiC bulk crystals is not available and the material quality of 3C SiC heteroepitaxially grown on Si is poor.

These make further advancement in 3C-SiC devices difficult. The availability and quality of reproducible single crystal wafers in 4H- and 6H-SiC, make these polytypes the most promising materials for the devices in some application area. The physical and electrical properties for these three common polytypes and Si at room temperature are listed in Table 1-1 for comparison.

In 4H-SiC, the carrier mobility is substantially higher compared to 6H SiC [1.4], which make the 4H polytype to be the most suitable choice for most SiC electronic devices. In addition, the inherent mobility anisotropy that degrades conduction parallel to the crystallographic c-axis in 6H-SiC [1.4] makes 4H-SiC more favorable for vertical power devices. The availability of higher mobility 4H-SiC single crystal substrate has largely overshadowed the progress made in obtaining improved 3C-SiC heteroepitaxilly grown on low-tilt-angle 6H-SiC substrates [1.5]. The higher mobility and more isotropic nature of 4H-SiC properties compared to 6H-SiC has made 4H-SiC the polytype most popular in the current device research activity. Therefore, the work in this thesis has been done on 4H-SiC polytype.

Table 1-1. Material properties of Si, 3C-SiC, 6H-SiC, and 4H-SiC at 300 K [1.2].

Property (unite)	Si	3C-SiC	6H-SiC	4H-SiC
Dielectric constant	11.8	9.7	9.7	9.7
Energy bandgap(eV)	1.12	2.39	3.03	3
Critical Field (MV/cm)	0.3	1.5	3.2	3
Electron mobility (cm^2/Vs)	1400	750	370	800
Hole mobility (cm^2/Vs)	600	40	90	115
Electron saturation velocity ($\times 10^7$cm/s)	1	2.5	2	2
Thermal conductivity (W/cm K)	1.5	5	4.9	4.9

1.3. SiC power devices

Generally, all SiC devices can be classified into two categories: Semi-conducting and semi-insulating devices. The semi-conducting SiC power devices can also be categorized into power rectifiers and power switches, while semi-insulating-based devices comprise high power high frequency application devices, radio frequency transistors, as shown in Figure 1-2.

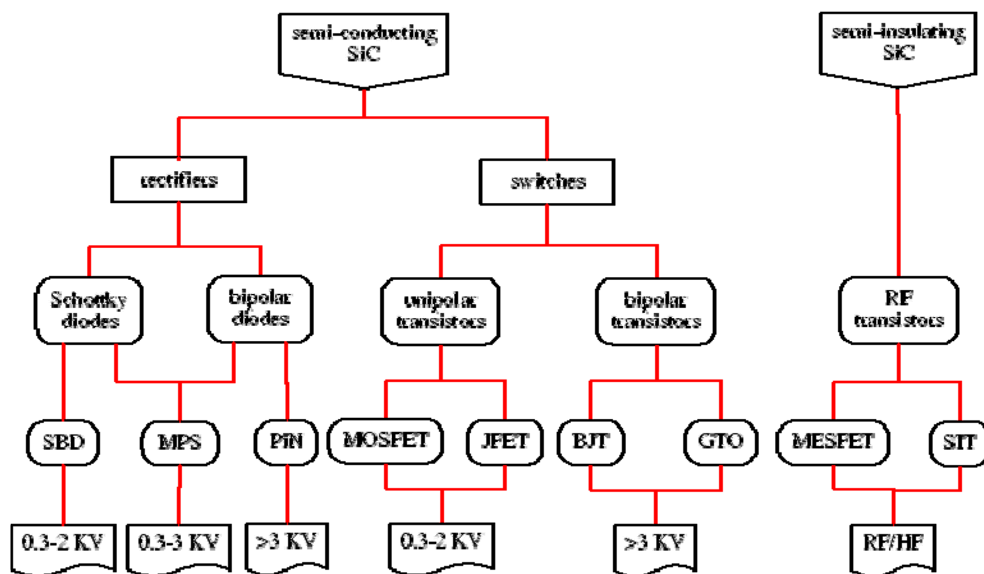

Figure 1-2. Summary of the Silicon Carbide electronic devices.

Many types of SiC power devices are still in the prototype demonstration phase while some have demonstrated performance far superior to silicon. These devices, which have demonstrated supereior performance, comprise the p-type intrinsic n-type (PiN) diodes, the Schottky barrier diode (SBD), the merged PiN Schottky diode (MPS) operating with

blocking voltages above 12 kV [1.6], the metal-oxide semiconductor field-effect transistor (MOSFET) [1.7], the junction field-effect transistor (JFET), the bipolar junction transistor (BJT) [1.8], the gate turn-off thyristor (GTO) with blocking ability over 3 kV and switch frequency over 60 HZ [1.9], the metal-semiconductor field-effect transistor (MESFET) and the static induction transistor (SIT) which demonstrate ultra high frequency, power density and an associated power added efficiency (PAE) of 78% [1.10]. The best repeated SiC power device performance is listed in Table 1-2.

Table 1-2 Best reported high voltage SiC devices.

Device	Polytype	Breakdown voltage (kV)	$R_{on,sp}$ ($m\Omega\text{-}cm^2$)	Group
Rectifiers				
SBD	4H	4.9	48	Purdue [1.11, 1.12]
PiN	4H	4.5	42	RPI [1.13]
PiN	4H	19.5	65	CREE [1.6]
JBS	4H	2.8	8	KTH-ABB [1.14]
MPS	4H	1.5	10	CREE [1.15]
Transistors				
UMOSFET	4H	5.05	105	Purdue [1.11]
UMOSFET	4H	3.06	121	Purdue [1.11]
DMOSFET	6H	1.8	46	SiCED [1.16]
DMOSFET	4H	2.4	42	CREE [1.17]
ACCUFET	4H	1.4	15.7	Purdue [1.11]
JFET	4H	5.5	218	CREE [1.18]
BJT	4H	1.8	10.8	CREE [1.8]
BJT	4H	0.5	50	Purdue [1.19]
GTO	4H	3.1	16.6	CREE [1.9]

1.4. Motivation for simulation improvements

Since the technology and research study in SiC devices are progressing rapidly, a good simulation methodology to predict performance of these devices will be very important

and useful for the industry and researchers in this area. In principle, ideal SiC device can be simulated in MEDICI [1.20], which is mostly used for Si device characteristics simulation. Several models with their default parameters are available in the simulator MEDICI. However, simulation of reverse characteristics of SiC pn junction using MEDICI becomes challenging as the ideal equilibrium minority carrier concentrations in SiC caused by wide bandgap are too low to yield meaningful minority carrier concentration for calculation of the reverse characteristics in simulator. In addition, due to the uncertainty of some parameters and high density of defects in SiC to be discussed in Chapter 2, which are not incorporated in the default model at all, the disagreement of simulation results with reported device characteristics [1.21] and reverse breakdown voltage is extremely large, as shown in Figure 1-3. Some work has been done on the simulation of 6H-SiC polytype [1.22] due to that most research activity were done for this polytype at first, while little work has been done on 4H-SiC in this area. There are more physical parameter measurement results available for 6H-SiC while there is less for 4H-SiC. In this thesis, the parameters with no conclusive measurement result will use Si default value in simulation.

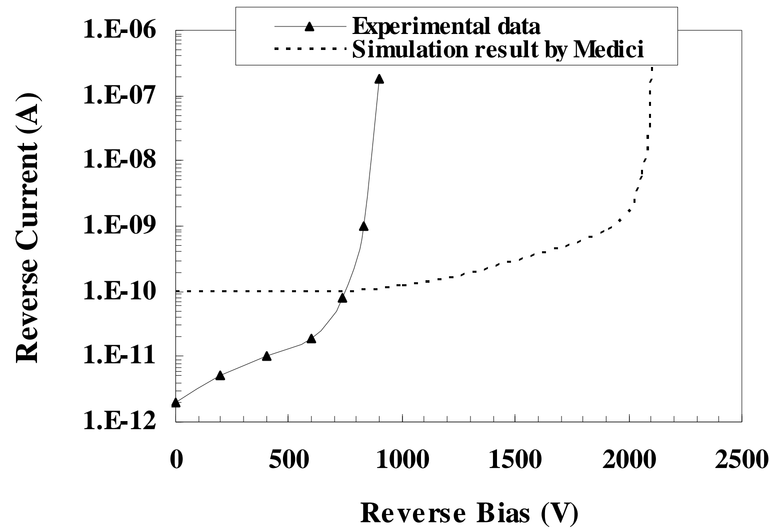

Figure 1-3. Comparison of reported experimental and simulation result of reverse characteristics of 4H-SiC pn diode [1.21]. The large difference shows that the simulation of practical SiC device needs improvement.

In this thesis, a reasonably accurate and predictive methodology to simulate 4H-SiC pn junction diodes, applicable to a wide variety of 4H-SiC pn diodes with varying doping concentration and junction depth will be introduced. This study will pave the way for simulation of SiC MOSFETs and other devices in their conducting and blocking regions of operation state.

1.5. Thesis outline

This thesis aims to present a thorough study on the improvement of simulation of practical 4H-SiC pn junction diodes. It covers both the physical study and simulation of practical 4H-SiC pn junction diodes containing defects. It is organized into six chapters, as follows:

Chapter 1 introduces material advantages of SiC and reviews the current SiC devices.

The motivation of the work is presented.

Chapter 2 presents the review of the process technology and theoretical analysis of the defects induced by the fabrication process in practical 4H-SiC pn junction diodes, which form the physical background for the work done in this thesis.

Chapter 3 describes and summarizes of the models and parameters for 4H-SiC device simulation in MEDICI. The defects discussed in Chapter 2 will be modeled with the models and parameters available in MEDICI.

Chapter 4 develops and verifies a reasonably accurate and predictive methodology to simulate the reverse characteristics of practical 4H-SiC pn junction diodes with varying doping concentration and junction depth, which will pave the way for simulation of SiC MOSFETs and other devices in their reverse-bias state. The physical background for the simulation methodology will also be discussed.

Chapter 5 develops and verifies a reasonably accurate and predictive methodology to simulate the forward characteristics of practical 4H-SiC pn junction diodes with varying doping concentration and junction depth. The physical background for the simulation methodology will also be discussed.

Chapter 6 draws the conclusion of this work and suggests some recommendations for future work.

Chapter 2

Current process technology

Silicon carbide has shown superior trend in high power, high temperature and high frequency application area since early 1950s. However, the fabricated devices show large deviation from the ideal characteristics. Many devices are still in the prototype demonstration phase. The main reasons are the immaturity of the fabrication process and the various defects induced by these process techniques. In this chapter, the main process technology for SiC material and the defects induced by these techniques are reviewed.

2.1. SiC bulk growth technology

2.1.1. History of Bulk growth of SiC wafers

SiC was predicted by Shockley to replace Si semiconductor material in the early 1950s [2. 1] because of its excellent material properties compared with Si. Reproducible wafers of reasonable consistency, size and quality are a necessity for commercial mass production of semiconductor electronic integrated circuit. However, the difficulty in producing large-size SiC single crystal wafers had made it impossible for SiC to even take over a small part of market from Si. Advanced SiC single crystal growth technology developed in the 1980s has revitalized the research activity of SiC electronic device. Now commercial availability of 2-, 3- and even 4-inch wafers have made SiC technology a commercial reality.

Many semiconductor materials can be melted and recrystallized into large single-crystals with the assistance of a seed crystal in manufacturing silicon wafers. This technology enables the mass-production of large size wafers. However, SiC sublimes instead of melting under certain attainable pressures in the conventional melt-growth techniques. Therefore, SiC can not be grown by the conventional techniques, which held back the realization of SiC crystals for mass production

Prior to 1980, experimental SiC electronic devices were limited on the small, irregularly shaped SiC crystal platelets grown as a by-product of the Acheson process for manufacturing industrial abrasives [2.2] or by the Lely process [2.3]. In the Lely process, SiC sublimes from polycrystalline SiC at temperatures near 2500℃ and randomly condenses on the walls of a cavity forming small-hexagonally shaped platelets. The crucible in which this process takes place is shown in Figure 2-1. These small, non-reproducible crystals provided the base for some basic SiC electronics research activity. However, it is common that there are mixed polytypes within a platelet. They were clearly not suitable for semiconductor mass production until the late 1970s.

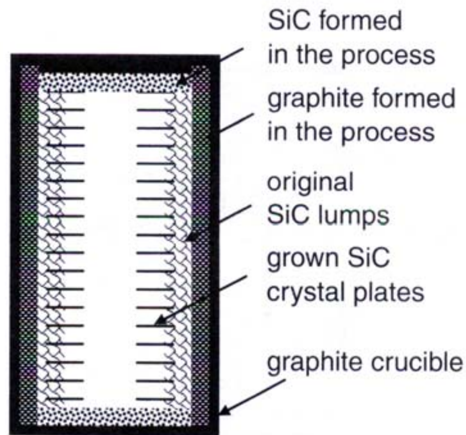

Figure 2-1. A schematic of a crucible in Lely process for crystal growth

2.1.2. Seeded sublimation growth technology

The difficulty in controlling the polytypes in Lely process is overcomed in the seeded sublimation growth or the modified Lely process by Tairov and Tsvetkov [2.4] in the late 1970s. The seeded sublimation technique refers to heating polycrystalline SiC source to sublime in a crucible similar to the one used by Lely process, and subsequently condense onto a cooler SiC seed crystal. This technique produces single crystal wafers for SiC successfully and is preferred for bulk crystal growth.

The typical equipment used for seeded sublimation growth consists of a water-cooled quartz reactor enclosure, surrounding the graphite crucible, in which the process takes place. The crucible is heated by radio frequency induction to about 1800～2400℃. The volatile species of polycrystalline SiC source material will evaporate and condense on the seed substrate. The seed can be arranged either to the lid of the crucible by clamping or gluing, or to the bottom of the crucible, as shown in Figure

2-2. The substrate forms a template for crystal growth, and a single crystal grows on the substrate according to the template.

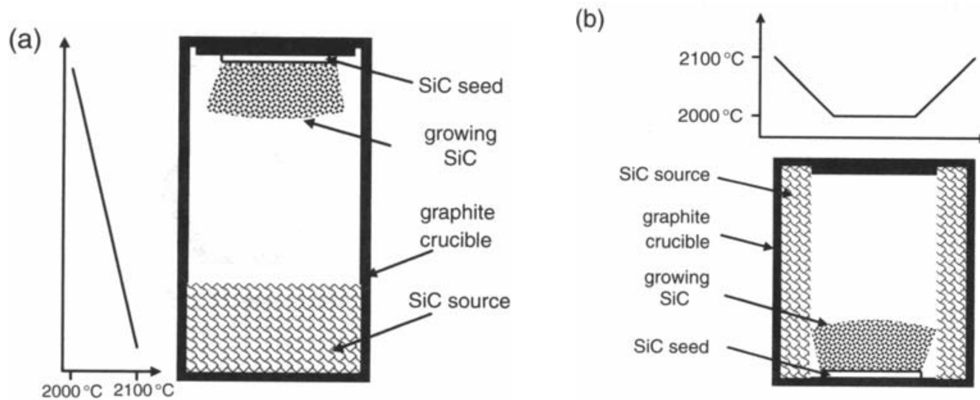

Figure 2-2. Cross section of crucibles for modified Lely process and typical temperature profile. (a).Lid mounting of the seed. (b) Bottom mounting of the seed

2.1.3. Commercial SiC wafers

Of the numerous polytypes of SiC, initial work focused on 3C-SiC polytype. However, it turns out the 3C-SiC single crystal wafer can only achieve poor quality while the quality of reproducible single crystal wafers in 4H and 6H-SiC is very good, which make these polytypes the most promising materials for SiC devices.

In 1989, Cree, Inc. became the first company to sell 25 mm diameter semiconductor wafers of 4H- and 6H- SiC [2.5]. The development of the seeded sublimation growth technique makes large and reproducible single crystal SiC wafers available, which enables SiC electronics development to take place since 1990. Now in bulk growth of 4H- and 6H-SiC, the initial problems with inclusions of foreign polytypes are basically solved, the doping concentration can be controlled over a wide range and the

defect concentration is steadily decreasing, though more efforts are still needed for further improvement of the defects density.

2.1.4. Bulk crystal defects

For cubic crystal like Silicon, three Miller indices, hkl, are used to describe directions and planes in the crystal. These are integers with the same ratio as the reciprocals of the intercepts with the x, y and z axes, respectively. For hexagonal crystal structures such as 4H-SiC, four principal axes are commonly used: a_1, a_2, a_3 and c, as shown in Figure 2-3. Only three are needed to identify a plane or direction, since the sum of the reciprocal intercepts with a_1, a_2 and a_3 is zero. For example, the three vectors a_1, a_2 and a_3 are all in the plane (0001).

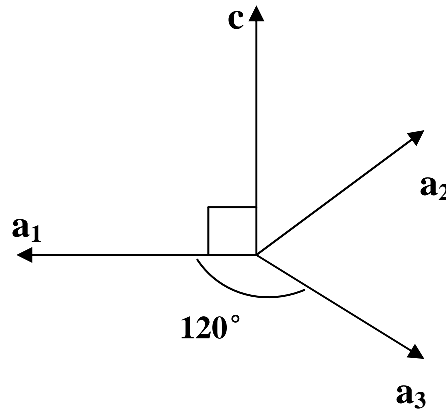

Figure 2-3. Principal axes for hexagonal crystal

Despite of a major development effort on seeded sublimation growth, process limitations still exist. These originate from the impurity and defect concentration in the crystals, the non-uniformity within the crystal and the stress within the substrates. The temperature distribution during the seeded sublimation growth should be

homogeneous to reduce the thermal stress in the crystal. The level of impurities determined by the purity of the ambient gas, of the source and of the crucible material can be improved to a certain degree.

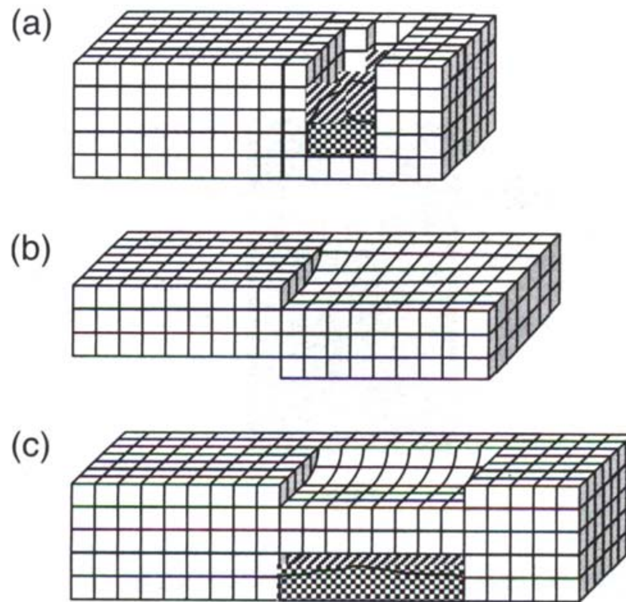

Figure 2-4. Possible defects a) Inclusion giving rise to a hollow core; b) Screw dislocation c) Inclusion giving rise to two screw dislocations of opposite sign.

Possible defects induced by the bulk growth are shown in Figure 2-4. The low stacking fault energy leads to the high probability of forming lattice defects and inclusions of different polytypes. The inclusions will degrade the performance of the device greatly. Therefore, polytype control is an important issue in one bulk growth. This technology relates to control the small difference in formation energies between the polytypes in SiC, and control that the (0001) lattice planes, on which most growth is performed, do not contain the unwanted polytype. The exposed surface of the seed and the growth conditions are usually more important parameters to control the

polytype of the grown crystal, than the bulk polytype of the seed itself. Growth on the $(1\underline{1}00)$ or $(11\underline{2}0)$ planes has also proven successful, as the polytype of the perfectly matches the seed. This process also has the advantage that micropipes do not propagate perpendicular to the c-axis, and hence the crystals are free from micropipes. The main draw back is that the preferred (0001) oriented substrates must be cut perpendicular to the boule, with a loss of material. Recently the density of polytype inclusions has been greatly reduced to less than 5 cm^{-2}.

2.2. SiC epitaxial growth technology

2.2.1 General Epitaxial growth technology of SiC

Nowadays, several techniques for forming epitaxial layers in SiC are used, which are vapor phase epitaxy, hot-wall epitaxy, sublimitation epitaxy, liquid-phase epitaxy, molecular beam epitaxy, and chemical vapor deposition (CVD) [2.6]. Chemical vapor deposition (CVD) is the only technique that is used for commercial applications of SiC expitaxial growth for its merits of low-cost, reproducibility, high quality, and suitability for mass production.

The principle of the CVD process is to transport reactive compounds (precursors) by a carrier gas to a hot zone. Then the precursors will thermally decompose into atoms or radicals of two or more atoms which may diffuse and solidify onto a substrate and form an epitaxial film. The substrate is a piece of SiC single crystal in the desired orientation, which is kept in a quartz tube, as shown in Figure 2-5. The tube is

inductively heated with an RF coil to around 1450℃[2.7].

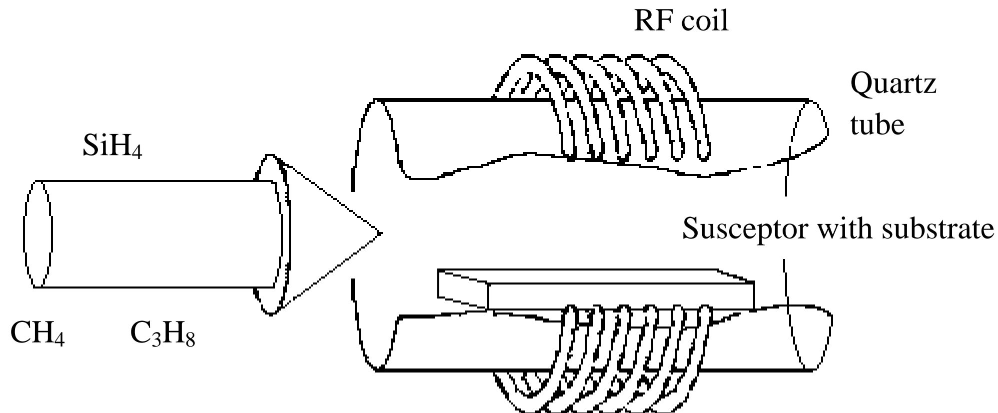

Figure 2-5. CVD setup for epitaxial growth of SiC [2.7].

Propane (C_3H_8) is used as the source of Carbon, Silane (SiH_4) is the source for Silicon, and Methane (CH_4) gas is used as the precursor for the reaction. At the given temperature, these radicals disassociate and form a homoepitaxial film on the surface of substrate on the graphite susceptor. This process continues until the desired thickness of an expitaxial layer has been grown.

2.2.2 High temperature CVD (HTCVD)

Several different types of CVD exist. The CVD in cold wall reactor, which was most commonly used in the past, is less frequently used and the CVD in hot wall reactor, known as HTCVD, has replaced it. The hot wall reactors have become increasingly popular due to the ability of obtaining high quality layer. This type of reactors made it possible to grow very thick, low-doped layers of good morphology and high quality, which are favorable for high voltage power devices. It also demonstrates a remarkably high uniformity in both thickness and doping.

In HTCVD, SiC CVD are carried out by heating SiC substrates in a chamber with flowing gases containing silicon and carbon that decompose and deposit Si and C onto the wafer allowing an epilayer to grow under well-controlled conditions. Conventional SiC CVD epitaxial growth processes are carried out at temperatures from 1450 to 1700 ℃ at about 0.1 to 1 atmosphere pressure, resulting in growth rates in the order of a micrometer per hour [2.8]. Higher-temperature (up to 2000℃) SiC CVD growth processes are being used to obtain higher SiC epilayer growth rates on the order of hundreds of micrometers per hour [2.9].

2.2.3. Epilayer crystal defects

The SiC epilayer surface morphology is greatly improved as refined substrate preparation and epilayer growth processes are developed. Many impurities and crystallographic defects which exist in seeded sublimation grown SiC wafers do not propagate into SiC epitaxial layers. Basal-plane dislocation loops from micropipes and screw dislocations in seeded sublimation grown SiC wafers are generally not observed in SiC epilayers. Unfortunately, however, screw dislocations (both micropipes and elementary screw dislocations) which exist in commercial c-axis wafers do replicate themselves along the crystallographic c-axis into SiC epilayers grown on wafers [2.10]. Therefore, devices in commercial epilayers are still subject to electrical performance and yield limitations induced by substrate screw dislocation defects.

Micropipes also known as hollow-core screw dislocation are major defects detrimental to high field devices. They propagate parallel to the c-axis and generate pipes through the SiC wafers. A device, which contains micropipes, shows glowing microplasma around the micropipes when breakdown takes place at the micropipes spot. And the breakdown voltage can be more than 50% lower than the bulk avalanche breakdown voltage. In the past few years, the density of micropipes in SiC wafers has been successfully reduced to less than 30 cm^{-2}. One-inch micropipe-free wafers and 2-inch wafers with micropipe density as low as 1.1 cm^{-2} have been demonstrated [2.11].

Elementary screw dislocations, also known as close-core screw dislocations, are formed from screw dislocations with a small Burgers vector. The difference between elementary screw dislocations and micropipes is the core of the dislocations. Elementary screw dislocations have closed cores while micropipes have hollow cores. Elementary screw dislocations are reported as not as harmful as micropipes and inclusion in terms of the influence on bulk avalanche breakdown. The breakdown voltage reduction owing to elementary screw dislocations ranges from 10% to 30%. Besides, breakdown caused by elementary screw dislocations does not permanently damage devices. The density of elementary screw dislocations is several orders of magnitude higher than that of micropipes and inclusions. The density typically ranges from $10^3 cm^{-2}$ to $10^4 cm^{-2}$. Therefore, even though elementary screw dislocations are

less harmful than micropipes, their density makes them the most detrimental defects for SiC device today.

In addition, another defect at the moment subject to extensive study is the assumed deep intrinsic defects that give semi insulating properties to SiC material. Normally semi insulating properties can be obtained by introducing Vanadium. But in HTCVD process, low doped and semi-insulating material can be obtained without intentional introduction of deep impurities. The origin of the residual defects causing this is not fully understood but the presence of deeper defect such as the Si vacancy and the UD1 defect states has been observed using FTIR and PL spectroscopy. Some samples with a dominating UD1 defect are thermally stable even up to a high annealing temperature of 1600 ℃.

2.3. Ion implantation and annealing in SiC

2.3.1 Ion implantation in SiC

In semiconductor fabrication process, ion implantation is the key technology for doping, especially for SiC. In SiC, thermal diffusion of the desired dopants is not applicable because of their extremely low diffusivities at temperatures less than 1800℃, which makes ion-implantation the indispensable technique for selective area doping of SiC devices. The technique of shooting ions into SiC crystals is similar to the ion implantation used in other semiconductor processing. The difference is in dopant activation and re-crystallization.

In SiC, ion implantation is usually carried out at elevated temperatures (～500 to 1000℃) using a patterned high-temperature mask. The elevated temperature during implantation promotes some lattice self-healing during the implantation. After the irradiation with ions, the implanted atoms have occupied predominantly interstitial lattice sites. These interstitial atoms do not affect the electrical material properties as long as they are not part of more complicated defects. Silicon and carbon atoms are kicked out from their lattice positions. The kicked out silicon and carbon atoms reside mostly on interstitial lattice sites and leave vacant lattice places behind.

2.3.2. Defects induced by Ion implantation

The ion implantation will lead to the generation of damage destroying the crystal structure of SiC. The damage includes point defects caused by single collision cascades at low ion doses and complete amorphization at high enough doses. The postimplant annealing is necessary to restore the crystal structure and electrically activate the implanted dopants by positioning them to substitutional sites in the lattice.

In addition, the irradiation will create an intrinsic defect with associated bound excitons in the near bandgap region can sometimes also be seen in as-grown material. These defects have hole attractive potentials and are temperature stable, which are hard to be removed during annealing.

2.3.3. Annealing

To activate implanted atoms and reduce the induced damage, a thermal annealing step at a temperature of 1600 ℃ follows the irradiation step, which allows the re-crystallisation of the material. The interstitial doping atoms will compete with interstitial silicon and carbon for free lattice point. The atoms ending up at lattice points become electrically active. Impurities consisting of isolated dopant atoms, intrinsic defect centers and complexes of both are generated.

2.3.4. Defects induced by annealing

The knowledge of annealing SiC is still limited and high level of defects still exist in the annealed SiC material, which make the annealing process still a scientific challenge. The issues are illustrated (but not limited to) as the following:

a) SiC is a dense and stable material with a short bond length (about 1.9Å) and a high binding energy, as the atomic density is about twice that of Si. As a result, intrinsic point defects in SiC are anticipated to be more stable, exhibiting a high thermal stability.

b) In addition to interstitial configuration, implanted atoms can occupy either Si- or C-sites and substitutional placement on the correct position to act as shallow dopants is not as easy as in Si. And there are nonequivalent lattice sites of either cubic or hexagonal symmetry in the different polytypes.

c) For common dopants Al, B, N, and P, high-temperature post-implant annealing

(1400-1800℃) is required to reach a reasonable amount of electrical activation. At such temperatures, preferential evaporation of Si occurs and the surface morphology deteriorates, which limits the maximum annealing temperature that is used to repair the lattice damage and position the implant atoms into the electrically active substitutional lattice positions. To minimize some of these problems, different concepts have been applied, such as effective encapsulants (primarily AlN) for protection of the SiC surface [2.12] and annealing in CVD-reactors using Si overpressure. These concepts appear to be quite effective, at least up to 1700℃.

d) During recrystallization of amorphous layers polytype transitions can happen, which may cause dopant redistribution and deactivation. The polytype transformation is in itself useful and can be used to obtain unstrained heterostructures. However, it will be difficult in restoring the lattice quality back to the original level, if the implanted lattice damage is of near-amorphous level. Therefore, for optimized electrical activation of the dopants during implantation annealing in SiC, it is advantageous to suppress amorphization by performing the ion implantation at elevated temperatures.

Although a substantial part of the damage induced by implantation can be removed by 1200 ℃ annealing, annealing at temperatures higher than 1500℃ should be performed because of the high bonding strength of the SiC lattice in order to achieve reasonable electrical activation. At such elevated temperature the SiC crystal surface

may decompose due to selective out-diffusion of Si from the SiC material. Hence some method to allow high temperature annealing of SiC implants while suppressing the out-diffusion of Si from the surface is needed. In addition, higher annealing temperatures also cause extended defects, such as dislocation loops, similar to the end of range defects seen in implanted and annealed Si. This imposes further limits on the annealing temperature.

2.4 Summary

In this chapter, the main reason that the disagreements of simulation results with reported device characteristics are quite large is identified as the immaturity of the fabrication process and the defects induced by these process techniques. The main process techniques for SiC pn junction diode is studied in this chapter, such as bulk and epitaxial growth, ion implantation and annealing process. Defects induced by these techniques are analyzed in details. Based on the study of the defects most likely to be induced by each process, the main defect affecting the SiC device performance is analyzed to be elementary screw dislocation.

Chapter 3

Models and Parameters for 4H-SiC Electrostatic Simulation

Numerical device modeling and simulation is a necessary tool for analyzing and developing semiconductor devices. This chapter will introduce the models and parameters for 4H-SiC device simulation. It will start with a brief introduction of MEDICI. Secondly, reviews of models in simulator and recently published material parameters of 4H-SiC applicable to MEDICI will be elaborated. Finally, the defects discussed in Chapter 2 will be modeled with the models and parameters available in MEDICI.

3.1 Introduction of MEDICI

Simulation tools help device community to gain an increased understanding of the device operation and provide the ability to predict electrical characteristics and behavior of the device. With the help of simulation tools, a better structure will be designed, device performance will be estimated, worst case analysis will be performed, and device parameters will be optimized to yield the best device performance. The increased availability of low-cost, high performance computing has made simulation widely used by device designer. To simulate semiconductor devices, MEDICI is commonly used as a two-dimensional (2D) simulation tool.

MEDICI is a widely used device simulation program. It can be used to simulate the behavior of MOS and bipolar transistors and other semiconductor devices. MEDICI models the two-dimensional (2D) distributions of potential and carrier concentrations in a device. And it can be used to predict electrical characteristics for arbitrary bias conditions. The program solves Poisson's equation and both the electron and hole current continuity equations in general semiconductor devices such as diodes and bipolar transistors and also the effects in which the current flow involves both carriers. MEDICI also analyzes unipolar devices, in which current flow is dominated by a single carrier, such as MOSFETs and JFETs.

MEDICI analyzes the device by solving numerically the following five basic equations:

- Poisson's equation, which will govern the electrical behavior of semiconductor devices:

$$\varepsilon\nabla^2\psi = -q(p - n + N_D^+ - N_A^-) - \rho_s \tag{3.1}$$

- Continuity equations for electrons and holes, which will also govern electrical behavior:

$$\frac{\partial n}{\partial t} = \frac{1}{q}\vec{\nabla}\cdot\vec{J}_n - (U_n - G_n) = F_n(\psi, n, p) \tag{3.2}$$

$$\frac{\partial p}{\partial t} = \frac{1}{q}\vec{\nabla}\cdot\vec{J}_p - (U_p - G_p) = F_p(\psi, n, p) \tag{3.3}$$

- Boltzmann transport theory, from which $\vec{J}_n$ and $\vec{J}_p$ in (3.2) and (3.3) can be written as:

$$\vec{J}_n = -q\mu_n n\vec{\nabla}\phi_n \quad (3.4)$$

$$\vec{J}_p = -q\mu_p p\vec{\nabla}\phi_p \quad (3.5)$$

Alternatively, $\vec{J}_n$ and $\vec{J}_p$ in (3.2) and (3.3) can be written in functions of ψ, n and p, with drift and diffusion components:

$$\vec{J}_n = -q\mu_n n\vec{E}_n + qD_n\vec{\nabla}n \quad (3.6)$$

$$\vec{J}_n = -q\mu_p p\vec{E}_p + qD_p\vec{\nabla}p \quad (3.7)$$

where p and n are hole and electron concentrations respectively, N_D^+ and N_A^- are the ionized donor and accepter concentrations respectively, ε is the dielectric permittivity, ψ is the intrinsic Fermi potential, ρ_s is a surface charge density that may be present due to fixed charge in insulating materials or charged interface states, $\vec{J}_n$ and $\vec{J}_p$ are vectors of the electron and hole current density respectively, U_n and U_p are the electron and hole recombination rates respectively, μ_n and μ_p are the electron and hole mobilities respectively, ϕ_n and ϕ_p are the electron and hole quasi-Fermi potentials respectively, and D_n and D_p are the electron and hole diffusivities respectively.

MEDICI uses the finite element method to solve the five basic device equations. According to the finite element method, the simulated device is discretized into simulation grids. The five basic device equations are solved on these simulation grids. This discretization process yields a set of coupled nonlinear algebraic equations which are to be calculated for a number of grid points with the different potentials and free-carrier concentrations.

This set of coupled nonlinear algebraic equations must be solved by a nonlinear iteration method. Two iteration methods, Gummel's and Newton's method are available in MEDICI. No matter which iteration method is used, the solutions will be carried out over the entire grid until a self-consistent potential (ψ) and free-carrier concentrations (*n, p*) are achieved. Once the potentials (ψ) and free-carrier concentrations (*n, p*) have been calculated at a given bias, it is possible to obtain the quasi-Fermi levels (ϕ) and the hole and electron currents ($\vec{J}_n$ and $\vec{J}_p$) from (3.4) – (3.5). This is how MEDICI basically simulates the device operation and obtains the data about the characteristics of the device.

The physical models and parameters used in MEDICI are critical for the results of device simulations. A number of physical models are incorporated in MEDICI for device simulations according to the characteristics of the semiconductor materials, such as lifetime, generation, recombination, photogeneration, impact ionization, energy bandgap narrowing, trap and mobility. Moreover, MEDICI also supports a number of semiconductor materials including SiC besides the most commonly used material Si.

All models and material parameters can be checked out in MEDICI manual and modified through statements in the input file for a specified region. The quantitative simulation of a device relies heavily on applicable device models and the values of the

parameters. For Si, better models and reasonably accurate parameters are available in MEDICI. For SiC, although several models with their default parameters are available in MEDICI, some of their default parameters do not provide realistic characteristics of SiC because of the limitation of the research progress; especially SiC material has many polytypes, resulting difference parameter values. This thesis will introduce some of the improvements for better realistic simulation of SiC device by adjusting the parameters and incorporating new models, which will be elaborated in chapter 4 and 5. Before embarking on the exercise of parameter changes, the physical models and parameter available for SiC will be summarized in the following sections so that the approach will be clear and complete.

3.2 Intrinsic Carrier Concentration and Energy Bandgap

In semiconductors, the electron and hole concentrations are defined by Fermi-Dirac distributions and a parabolic density of states. When these are integrated, we can get:

$$n = N_C F(\eta_n) \tag{3.8}$$

$$p = N_V F(\eta_p) \tag{3.9}$$

Based on above equations, the intrinsic carrier concentration can be obtained:

$$n_i(T) = \sqrt{N_C N_V}\, e^{-E_g/2kT} \tag{3.10}$$

Where N_C and N_V are calculated by

$$N_C(T) = N_C(300) \times \left(\frac{T}{300}\right)^{\frac{3}{2}} \tag{3.11}$$

$$N_V(T) = N_V(300) \times \left(\frac{T}{300}\right)^{\frac{3}{2}} \tag{3.12}$$

$N_C(300)$ and $N_V(300)$ are specified as **NC300** and **NV300** in MEDICI (user-specified parameters in MEDICI are written in capital and bold letters in this thesis), which can be modified from the default values through the material statement for different materials. From default values of MEDICI, **NC300** and **NV300** are 1.23 $\times 10^{19}$ cm^{-3} and 4.58 $\times 10^{18}$cm^{-3} respectively, which can be used for 4H-SiC simulation.

E_g is the band gap energy of the semiconductor, that is, $E_g = E_C - E_V$. Energy bandgap of 4H-SiC has been measured by absorption [3.1]. The value can be set as 3.26eV at 300K, which shows good agreement with the previous data in [3.2]. To simulate 4H-SiC device, **EG. MODEL** on Material statement should be specified to be 1, which means the following expression is chosen to calculate temperature dependency of the energy bandgap in MEDICI:

$$E_g(T) = E_g(300) + \alpha \times (\frac{300^2}{300+\beta} - \frac{T^2}{T+\beta}) \tag{3.13}$$

For 4H-SiC simulation, $E_g(300)$ (**EG300**, Bandgap energy at 300K) can be set as 3.26eV. α and β (**EGALPH and EGBETA**) are formula constants, which are 4.59×10^{-4} eV/K and 530 K for 4H-SiC, instead of the default value 4.73×10^{-4} eV/K and 636 K, respectively. The intrinsic carrier concentration as a function of temperature for 4H-SiC and Si are shown in Figure 3-1.

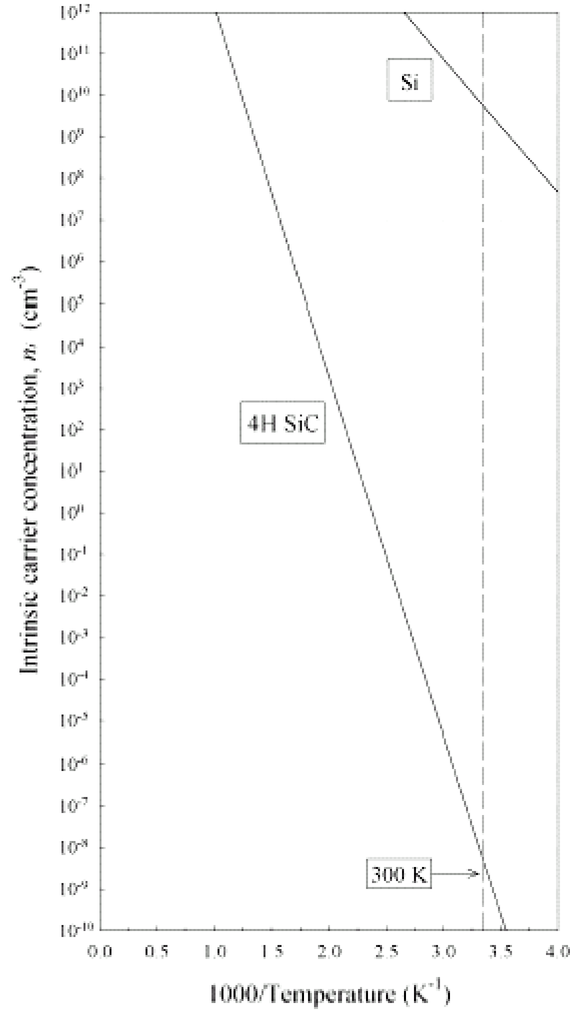

Figure 3-1. Intrinsic carrier concentration for 4H SiC and Si VS Temperature [3.3].

Usually at high doping levels, the interaction between carriers and overlap of the electron wave functions will affect the value of energy bandgap [3.4] greatly. Bandgap narrowing effects due to heavy doping are included as spatial variations in the intrinsic concentration [3.5], which leads to the change of the electric field in the transportation of carriers due to intrinsic Fermi potential. MEDICI takes the bandgap narrowing effect into account as follows:

$$\nabla E_g = \frac{V_0 \cdot q}{2kT}[\ln \frac{N_{total}(x,y)}{N_0} + \sqrt{(\ln \frac{N_{total}(x,y)}{N_0})^2 + C}] \tag{3.14}$$

$$n_{ie}(x, y) = n_i \exp(\nabla E_g) \qquad (3.15)$$

V_0, N_0 and C (**V0.BGN**, **N0.BGN**, and **CON.BGN**) are constant parameters, which can be adjusted from the default values in MEDICI. In the simulation of 4H-SiC semiconductor device, the default value in MEDICI will be used. **V0.BGN**, **N0.BGN**, and **CON.BGN** are 9×10^{-3} V, 1.0×10^{17} cm^{-3} and 0.5, respectively.

3.3 Carrier Mobility

In semiconductor device, the theoretical *I-V* characteristics strongly depend on physical mobility models and velocity saturation models. The carrier mobilities μ_n and μ_p account for the various scattering mechanisms and effects in carrier transport. The carrier mobilities μ_n and μ_p are a function of the total doping concentration, the temperature, and the magnitude of electric fields. Lattice scattering (acoustic phonons) and ionized impurity scattering, together with anisotropic scattering [3.6], are the most important mechanisms which will limit the mean free path of carriers at low electric fields in SiC [3.7, 3.8, 3.9]. Since free carrier mobility is affected greatly by the value of electric field, the mobility model in MEDICI is composed by low field and high field mobility components.

3.3.1 Low field mobility

For low field mobility, concentration and temperature dependent empirical mobility functions for silicon given by the Caughey-Thomas equation [3.10] can be selected for simulating 4H-SiC material. At room temperature, these are given by the

expressions:

$$\mu_{0n} = \mu_{\min,n} + \frac{\mu_{\max,n} - \mu_{\min,n}}{1 + (\frac{N_{total}}{N_{ref,n}})^{\alpha_n}} \tag{3.16}$$

$$\mu_{0p} = \mu_{\min,p} + \frac{\mu_{\max,p} - \mu_{\min,p}}{1 + (\frac{N_{total}}{N_{ref,p}})^{\alpha_p}} \tag{3.17}$$

where N_{total} is the local total impurity concentration, The parameters $\mu_{\max,n}$ and $\mu_{\max,p}$ (**MUN.MAX** and **MUP.MAX**) are the mobilities of undoped or unintentionally doped samples, where lattice scattering is the main scattering mechanism, while $\mu_{\min,n}$ and $\mu_{\min,p}$ (**MUN.MIN** and **MUP.MIN**) are the mobilities in highly doped material, where ionized impurity scattering is dominant. The parameters $N_{ref,n}$ and $N_{ref,p}$ (**NREFN** and **NREFP**) are the doping concentrations at which the mobility is between $\mu_{\max}$ and $\mu_{\min}$. The parameters α_n and α_p (**ALPHAN** and **ALPHAP**) are the measure of how quickly the mobilities switch from $\mu_{\max}$ and $\mu_{\min}$. This analytic mobility model can be specified with the **ANALYTIC** parameter on the **MODELS** statement. For 4H-SiC simulation, the values for these parameters are summarized in Table 3-1. The data are coming from Medici Technical support, which are universally used parameters for 4H-SiC simulations to date, summarized and updated by Japanese researchers. Currently different experiment data are obtained for one parameter, this data list has chosen the best result from these data and is applicable to 4H-SiC simulations.

Table 3-1. Parameters of low field mobility for 4H-SiC at 300K.

Parameters	Values for 4H-SiC
MUN.MAX	947.0 cm^2/Vs
MUP.MAX	124.0 cm^2/Vs
MUN.MIN	0.0 cm^2/Vs
MUP.MAX	15.9 cm^2/Vs
NREFN	1.94×10^{17} cm^{-3}
NREFP	1.76×10^{19} cm^{-3}
ALPHAN	0.61
ALPHAP	0.34

3.3.2 High field mobility

When the electric field is high enough, the carrier velocity will be no longer proportional to the field, and thus no longer can be described by a field independent mobility. Field-dependent mobility model is developed to account for carrier heating and velocity saturation effects. The saturated drift velocity is a consequence of scattering mechanisms such as optical phonon scattering, phonon dispersion, phonon absorption as well as emission, and the energy band non-parabolicity [3.11]. The high field mobility model is based on the low field mobility model with further extensions to take the high field effects into account.

The high field mobility model is given in an analytical expression as a function of the saturation velocity and electric field in the direction of current flow. The expression is as follows:

$$\mu(E) = \frac{v_d(E)}{E} \tag{3.18}$$

The effect of parallel field on the low drift electron mobility model as described in (3.16) and (3.17) can be expressed as following equations, which are used for modeling the mobility field dependence of Si [3.10]:

$$\mu_n = \frac{\mu_{S,n}}{[1 + (\frac{\mu_{S,n} E}{V_{sat,n}})^{\beta_n}]^{\frac{1}{\beta_n}}} \tag{3.19}$$

$$\mu_p = \frac{\mu_{S,p}}{[1 + (\frac{\mu_{S,p} E}{V_{sat,p}})^{\beta_p}]^{\frac{1}{\beta_p}}} \tag{3.20}$$

where $\mu_{S,n}$ and $\mu_{S,p}$ are the low field mobilities which may include the scattering mechanisms, $V_{sat,n}$ and $V_{sat,p}$ (**VSATN** and **VSATP**) are the saturation velocities, and β_n and β_p (**BETAN** and **BETAP**) are constants that influence how quickly the velocity rises up to saturation. E is the electrical field parallel to the current flow.

The knowledge about the high-field mobility of SiC is still limited. The only experimental result was published by Khan and Cooper [3.12, 3.13]. They measured the drift velocity (n-doped at about 10^{17} cm^{-3}) was measured as a function of electric field in 4H-SiC epilayers. All experimental results are referring to a current flow perpendicular to the c-axis. The parameters used for 4H-SiC simulation are shown in Table 3-2 and Figure 3-2.

Table 3-2. Parameters of high field mobility for 4H-SiC at 300K and 593K [3.3]

Parameters	Values for 4H-SiC at 300K	Values for 4H-SiC at 593K
$\mu_{S,n}$	450 cm^2/Vs	130 cm^2/Vs
VSATN	2.2×10^7 cm/s	1.6 cm/s
BETAN	1.2	2.2
$\mu_{S,p}$	450 cm^2/Vs	130 cm^2/Vs
VSATP	2.2×10^7 cm/s	1.6×10^7cm/s
BETAP	1.2	2.2

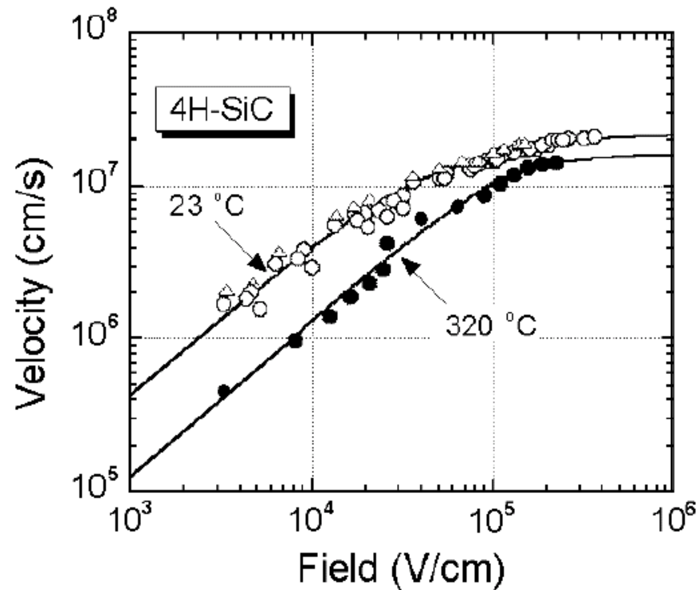

Figure 3-2. Drift velocity of electron in 4H SiC as functions of the applied field [3.3]

3.3.3 Anisotropy in Mobility

In 4H-SiC polytype, the carrier transport properties exhibit an anisotropic behavior with regard to crystallographic orientation. In the wafer fabrication, 4H-SiC substrates are usually cut perpendicular or offset a few degrees to the c-axis of the crystal. Therefore, one should be aware that the carrier mobility is either perpendicular to the

c-axis (in direction of the basal of the crystal) or parallel to the c-axis, depending on the device structure and operation.

Experimental measurements of the electron mobility anisotropy in N-type 4H-SiC using the Hall Effect and through MC calculations have been studied in [3.14, 3.15,3.16]. These studies show an agreement of a ratio value of $\mu_{(1120)} / \mu_{(0001)} \approx 0.83$ for 4H-SiC, which is temperature independent [3.12].

In (3.19) and (3.20), the high field mobility model shows the dependence of carrier mobility on the component of electric field in the direction of the current flow. Due to anisotropy of 4H-SiC material, the effects caused by anisotropy to the mobility should be included in the device modeling. In MEDICI, the so-called Anisotropic Material Advanced Application Module (AM-AAM) can be used to account for the anisotropy nature in 4H-SiC materials. To model the anisotropic mobility, the expression is given as:

$$\underline{\underline{\mu_n}} = \begin{pmatrix} \mu_{n_{xx}} & 0 & 0 \\ 0 & \mu_{n_{yy}} & 0 \\ 0 & 0 & \mu_{n_{zz}} \end{pmatrix} = \mu_{n_{mat}} \cdot \begin{pmatrix} \mu_n(1) & 0 & 0 \\ 0 & \mu_n(2) & 0 \\ 0 & 0 & \mu_n(3) \end{pmatrix} \tag{3.21}$$

$$\underline{\underline{\mu_p}} = \begin{pmatrix} \mu_{p_{xx}} & 0 & 0 \\ 0 & \mu_{p_{yy}} & 0 \\ 0 & 0 & \mu_{p_{zz}} \end{pmatrix} = \mu_{p_{mat}} \cdot \begin{pmatrix} \mu_p(1) & 0 & 0 \\ 0 & \mu_p(2) & 0 \\ 0 & 0 & \mu_p(3) \end{pmatrix} \tag{3.22}$$

Because the studied mention above are all done on N-type 4H-SiC, no available experimental data is available for the hole anisotropic mobility, the default values of which will be used in simulation. To simulate of 4H-SiC, $\mu_n(1), \mu_n(2)$and $\mu_n(3)$ (**MU.N(1)**, **MU.N(2)** and **MU.N(3)**) are set to be 0.83,1 and 0.83, respectively.

3.4 Generation and Recombination

MEDICI models generation and recombination processes within the quasi-static approximation according to various physical mechanisms. All the models to be explained in this part evaluate the recombination rate. The rates will be summed to obtain the overall recombination rate for the corresponding carrier type. Both eternal optical generation and the band-to-band processes induced by defects can account for auger recombination and impact ionization. When the overall rates are positive, they refer to recombination, and when they are negative, they refer to generation.

The overall recombination rate is:

$$U = U_n = U_p = U_{SRH} + U_{Auger} + U_{dir} \tag{3.23}$$

3.4.1 Shockley-Read-Hall Recombination

The Shockley-Read-Hall (SRH) rate [3.17] is obtained from the balance equation for each generation-recombination center within the quasi-static approximation. The characteristics of each generation-recombination center vary with different process technology. Therefore, there are several quantities like the effective electron and hole lifetimes, which give rise to one effective single-level SRH rate:

$$U_{SRH} = \frac{pn - n_{ie}^2}{\tau_p[n + n_{ie}\exp\frac{E_{trap}}{kT}] + \tau_n[p + n_{ie}\exp\frac{E_{trap}}{kT}]} \tag{3.24}$$

The parameter E_{trap} (**ETRAP**) represents the difference between the trap energy level and the intrinsic Fermi level:

$$E_{trap} = E_t - E_i \tag{3.25}$$

In (3.24), n_{ie} is the effective intrinsic concentration. τ_n and τ_p are the electron and hole lifetimes, which may be concentration dependent.

$$\frac{\tau_{0n}}{\tau_n} = A_n + B_n(\frac{N_{total}}{N_{SRH,n}}) + C_n(\frac{N_{total}}{N_{SRH,n}})^{E_n} \tag{3.26}$$

$$\frac{\tau_{0p}}{\tau_p} = A_p + B_p(\frac{N_{total}}{N_{SRH,p}}) + C_p(\frac{N_{total}}{N_{SRH,p}})^{E_p} \tag{3.27}$$

The default values of A_n, B_n, C_n, E_n, A_p, B_p, C_p and E_p in MEDICI can reduce (3.26) and (3.27) into

$$\tau_n = \frac{\tau_{0n}}{1 + N_{total} / N_{SRH,n}} \tag{3.28}$$

$$\tau_p = \frac{\tau_{0p}}{1 + N_{total} / N_{SRH,p}} \tag{3.29}$$

For simulation of 4H-SiC, the default values for Si are used. τ_{0n} and τ_{0p} (**TAUN0 and TAUP0**) are both 10^{-7}s. $N_{SRH,n}$ and $N_{SRH,p}$ (**NSRHN and NSRHP**) are both 5 $\times 10^{16}$ cm^{-3}.

3.4.2 Auger Recombination

The Auger process, which only happens at high carrier concentrations, involves three particles. The Auger recombination rate is proportional to the concentrations of the

respective reaction partners [3.18] as follows:

$$U_{Auger} = (nC_{Aug,n}(T) + pC_{Aug,p}(T))(pn - n_{ie}^2) \tag{3.26}$$

where $C_{Aug.n}(T)$ and $C_{Aug.p}(T)$ are the Auger coefficient of electrons and holes:

$$C_{Aug.n}(T) = A_n (\frac{T}{300})^{D_n} \tag{3.27}$$

$$C_{Aug.p}(T) = A_p (\frac{T}{300})^{D_p} \tag{3.28}$$

The values of the parameters in (3.28) have no available experimental results for 4H-SiC. Therefore, in the simulation of 4H-SiC device, the default values of these parameters for Si will be used.

3.4.3 Impact ionization

To understand of SiC power devices breakdown characteristics, it is important to have a clear understanding of impact ionization. Impact ionization is one of the most important factors which determines the maximum voltage that a device will sustain. The impact ionization can be considered as the reverse process to the Auger recombination [3.4]. A new electron-hole pair is generated by the impact of a high energy hole or electron on an electron in the valence band. The knocked out electron will generate more new electron-hole pair after being accelerated in a high electric field. Impact ionization is a non-equilibrium process which requires high electric fields.

The probability that electrons or holes will create electron-hole pairs is given by the product of impact ionization rate and the electron/hole concentration. The maximum

electric field and the breakdown voltage are determined by the impact-ionization rate for electron-hole pairs. Therefore, impact ionization rates are the key parameters to estimate the blocking ability of a power semiconductor device.

A first approximation of the breakdown voltage as function of doping was derived for various materials [3.19]. However, the result of critical field by putting SiC band gap into this approximation is much lower than it actually is [3.20]. Early report on measurements of the breakdown voltage as function of the doping and temperature for 4H-SiC was published by Palmour *et al*, who indicated negative temperature coefficient for breakdown in SiC [3.21].

However, more recent publication by Raghunathan *et al* indicated positive temperature and lower coefficients using the pulsed electron beam induced current (P-EBIC) technique [3.22]. Besides experimental problems, the deviations of the results might be caused by the presence of defects in the material. The experimental results for the ionization coefficient from Raghunathan *et al* measurements will be discussed in detail later in Chapter 4. Here the parameters set for simulation will be briefly addressed.

MEDICI can perform impact ionization analysis in two ways: post-processing method and self-consistent method. The generation rate for electron-hole pair due to impact ionization in both ways can be expressed as:

$$G^{II} = \alpha_{n,ii} \cdot \frac{\left|\vec{J}_n\right|}{q} + \alpha_{p,ii} \cdot \frac{\left|\vec{J}_p\right|}{q} \tag{3.29}$$

where $\vec{J}_n$ and $\vec{J}_n$ are the electron and hole current densities, and $\alpha_{n,ii}$ and $\alpha_{p,ii}$ are the electron and hole ionization coefficient, which can be express in terms of the electric field as:

$$\alpha_{n,ii} = N.IONIZA \exp[-(\frac{E_{n,ii}^{crit}}{E_n})^{EXN.II}] \tag{3.30}$$

$$\alpha_{p,ii} = P.IONIZA \exp[-(\frac{E_{p,ii}^{crit}}{E_p})^{EXP.II}] \tag{3.31}$$

where E_n and E_p are the effective driving fields for electrons and holes. In MEDICI default simulation, the critical fields can be expressed as

$$E_{n,ii}^{crit} = \frac{E_g(T,x)}{q\lambda_n(T)} \tag{3.32}$$

$$E_{n,ii}^{crit} = \frac{E_g(T,x)}{q\lambda_n(T)} \tag{3.33}$$

If **ECN.II** and **ECP.II** are specified, the critical field will be assigned with these values without the calculation of (3.32) and (3.33). To simulate 4H-SiC device, the parameters specified for the impact ionization model are listed in Table 3-3.

Table 3-3. Parameters of impact ionization model for 4H-SiC

Parameters	Values for 4H-SiC
N.IONIZA	1.66×10^{6} cm^{-1}
P.IONIZA	3.25×10^{6} cm^{-1}
ECN.II	1.273×10^{7} V/cm
ECP.II	1.71×10^{7} V/cm
EXN.II	1
EXP.II	1.568

3.4.4 photogeneration

In MEDICI, photogeneration model allows the simulation of the steady-state or time-dependent injection of electrons and holes into the device. The generation rate of photogeneration, which will apply to the continuity equation, depends on length, radial distance and time.

$$G_n(l,r,t), G_p(l,r,t) = L(l)\times R(r)\times T(t) \tag{3.34}$$

The time dependence represents how the photogeneration will change with time. It can assume one of the four functional forms, Gaussian, delta or uniform in equation (3.35).

$$T(t) = \begin{cases} \dfrac{2\exp\left[-\left(\dfrac{t-T_0}{T_c}\right)^2\right]}{T_c\sqrt{\pi}\,erfc\left(-\dfrac{T_0}{T_c}\right)} & Gaussian \\ \delta(t-T_c) & Delta \\ 1 & Uniform \end{cases} \quad (3.35)$$

The radial dependence represents the distribution of generated carrier concentration in horizontal direction. R_{char} is the characteristic radius of generated carrier concentration.

$$R(r) = \begin{cases} \exp[-(\dfrac{r}{R_{char}})^2] & R_{char} > 0 \\ 1 & R_{char} = 0 \end{cases} \quad (3.36)$$

The length dependence represents the distribution of generated carrier concentration in vertical direction, which has the following forms:

$$L(l) = A_1 + A_2 \times l + A_3 \times \exp(A_4 \times l) + k[C_1 \times (C_2 + C_3 \times l)^{C_4} + L_f(l)] \quad (3.37)$$

Parameters A_1, A_2, A_3 and A_4 (**A1**, **A2**, **A3**, and **A4**) can be used to describe the length dependence of the photogeneration rate. If carriers generated are defined to be of constant length dependence, parameters **A2**, **A3**, and **A4** which represent linear, pre-exponential and exponential length dependence of charge generation separately, are equal to zero. The value of parameter **A1**, which represents uniform carrier generation everywhere, will determine the carrier generation rate of photogeneration, and thus increase the carrier concentration in a device to which photogeneration is

applied.

In the simulation of SiC pn junction, there is the no breakdown problem for reverse simulation due to the low intrinsic carrier concentration at room temperature caused by the wide bandgap. When the simulator has to cope with the majority carrier concentration on the order of 10^{18}cm^{-3} and a minority carrier concentration of less than 10^{-18}cm^{-3}, the numerical accuracy is not sufficient, and it is hard to get a accurate result. To solve this problem, photogeneration can be applied to increase the carrier concentration at the pn junction at the beginning of the simulation. This approach is to be explained in detail in chapter 4.

3.5 Trap Model

In MEDICI, the Trapped Charge Advanced Application Module (TC-AAM) allows the simulation of semiconductor devices containing traps. The TC-AAM allows the analysis of important carrier trapping and de-trapping mechanisms within semiconductor materials.

To analyze traps, the energy bandgap is divided in up to 50 discrete energy levels E_{t_i} . Then, recombination and trapping processes in the semiconductor device are analyzed at each trap energy level.

For recombination, the Shockley-Read-Hall (SRH) model is used. Trapping processes

is also modeled using SRH model.

$$U = \sum_i \frac{pn - n_{ie}^2}{\tau_{p_i}[n + n_{t_i}] + \tau_{n_i}[p + p_{t_i}]} \tag{3.38}$$

$$n_{t_i} = n_{ie} \exp\left(\frac{E_{t_i}}{kT}\right) / D_d \tag{3.39}$$

$$p_{t_i} = n_{ie} \exp\left(-\frac{E_{t_i}}{kT}\right) / D_d \tag{3.40}$$

τ_{n_i} and τ_{p_i}, the carrier lifetimes for electrons and holes, are defined respectively as a function of bandgap energy. Their values can be calculated from the parameters **TAUN** and **TAUP** on the **TRAPS** statement. The parameter D_d (**DGEN**) accounts for degeneracy effects. The trap energy level E_{t_i} is specified relative to the intrinsic Fermi level. The effects of recombination including tunneling are also included for each trap energy level.

The following expression shows the trap occupation function for electron traps, where f has a maximum value of 1, indicating a completely full trap:

$$f_i = \frac{\tau_{p_i} n + \tau_{n_i} p_{t_i}}{\tau_{p_i}(n + n_{t_i}) + \tau_{n_i}(p + p_{t_i})} \tag{3.38}$$

Poisson equation, the self-consistent solution of the standard device equation, is modified to include the number of electrons that are trapped.

$$\varepsilon \nabla^2 \psi = -q(p - n + N_D^+ - N_A^- - \sum_i N_{t_i} f_i) - \rho_s \tag{3.39}$$

where ψ is the intrinsic fermi potential. N_D^+ and N_A^- are the ionized impurity concentrations. ρ_s is a surface charge density that may be present due to fixed

charge in insulating materials or charged interface states. N_{t_i} is the total number of traps for the i th energy level. N_{t_i} is obtained from the **N.TOTAL** parameter on the **TRAPS** statement and is also a function of energy and position. If the trap state is specified as **CHARGED**, then the following form of the Poisson equation should be used instead of (3.39).

$$\varepsilon\nabla^2\psi = -q(p - n + N_D^+ - N_A^- - \sum_i N_{t_i}(f_i - 1)) - \rho_s \tag{3.40}$$

If an electron trap level is specified to be charged, then an empty trap has a positive charge. If the electron trap is filled by an electron, then the positive charge of the trap will be compensated by the negative charge of the electron, and the net charge of the trap will become zero. If a hole trap level is specified as charged, then an empty trap has a negative charge. If the charged hole trap is filled by a hole, then the positive charge of the hole cancels the negative charge of the trap, and the net charge of the trap will become zero.

Because all of the defects discussed in chapter 2 will create traps in the bandgap, traps will be incorporated, to include the effect of the defects to the 4H-SiC pn junction, in the simulation work of this thesis. The trap energy and density can be specified in the trap model, which will be discussed in detail in chapter 5. Thus the simulation results are able to reflect the influence of defects on practical SiC device and the simulations of current practical SiC device are improved.

3.6 Summary

In this chapter, models of 2D numerical device modeling tool MEDICI are introduced for 4H-SiC device simulation. The physical models and parameters used in MEDICI are elaborated, such as generation, recombination, photogeneration, impact ionization, trap and mobility. Parameters available for 4H-SiC have been summarized in the each section. Two models should be specially incorporated in simulation of practical 4H-SiC pn junction diode, photogeneration and trap model. Photogeneration can be applied to increase the carrier concentration at the pn junction at the beginning of the simulation. Trap model will enable the simulation results to reflect the influence of defects on practical SiC device.

Chapter 4

Realistic Simulation of Reverse Characteristics of 4H-SiC pn Junction Diode

Due to the superior property of high critical field, about one order of magnitude higher than that of Si, SiC becomes a major candidate for high power device. A good simulation methodology to predict performance of these devices will be very useful for the industry and researchers in this area. In this chapter, a reasonably accurate and predictive methodology to simulate the reverse characteristics of 4H-SiC pn junction diodes with varying doping concentration and junction depth will be introduced. This study will pave the way for simulation of SiC MOSFETs and other devices in their forward- and reverse-bias state.

4.1 Reverse blocking ability and impact ionization in 4H-SiC pn junction

In order to fully understand the reverse characteristics of silicon carbide, it is necessary to investigate its impact ionization process and avalanche multiplications. Impact ionization is one of the most important factors which determines the maximum voltage that a device will sustain.

The impact ionization can be taken as the reverse process to the Auger recombination. A

new electron-hole pair is generated by the impact of a high energy hole or electron on an electron in the valence band. The electron will be knocked out, and generate more new electron-hole pair after being accelerated in a high electric field. Impact ionization is a non-equilibrium process which requires high electric fields.

The probability that electrons or holes will create electron-hole pairs is given by the product of impact ionization rate and the electron/hole concentration. The maximum electric field and the breakdown voltage are determined by the impact-ionization rate for electron-hole pairs. Therefore, impact ionization rates are the key parameters to estimate the blocking ability of a power semiconductor device. The theoretical quantitative calculation of reverse characteristics of 4H-SiC is now discussed as follows.

4.1.1. Basic equations

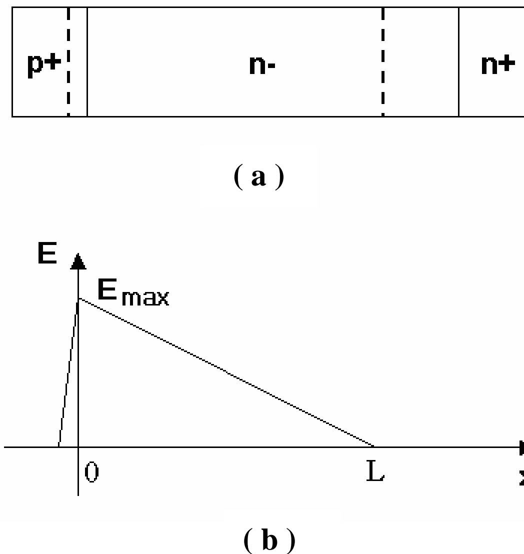

Figure 4-1: Electric field for normal p-i-n diode under reverse bias

In a p+/n- junction of power device, the ability to block current flow at high voltages is obtained by supporting the voltage across the pn junction with revere bias. It can sustain high voltage without undergoing catastrophic avalanche breakdown. Consider a normal parallel-plane, abrupt, p-i-n diode with a reverse bias of V_a applied. The electric field plot for this p+/n- junction under reverse bias is shown in Figure 4-1. The Poisson's equation in the n-region is given by:

$$\frac{d^2V}{dx^2} = -\frac{dE}{dx} = -\frac{Q(x)}{\varepsilon_{SiC}} = \frac{qN_D}{\varepsilon_{SiC}} \tag{4.1}$$

Where $Q(x)$ is charge in the depletion region due to the presence of ionized donors, ε_{SiC} is the permittivity of the silicon carbide, q is the electron charge, and N_D is the donor concentration on the doped n-region. An integration of (4.1) with the boundary condition that the electric field must decrease to zero at the edge (W) of the depletion region leads to a solution for the electric field distribution:

$$E(x) = \frac{qN_D}{\varepsilon_{SiC}}(W - x) = E_c - kx \tag{4.2}$$

where $k = \frac{qN_D}{\varepsilon_{SiC}}$.

An integration of the electric field through the depletion region with the boundary condition that the potential is zero in the p+ region leads to the potential distribution:

$$V(x) = \frac{qN_D}{\varepsilon_{SiC}}(Wx - \frac{x^2}{2}) \tag{4.3}$$

The potential in the depletion region varies from 0 in the p+ region to V_a at the edge of the depletion region.

$$W = \sqrt{\frac{2\varepsilon_{SiC} V_a}{qN_D}} \tag{4.4}$$

The maximum electric field occurs at x=0 for the abrupt junction:

$$E_{\max} = \sqrt{\frac{2qN_D V_a}{\varepsilon_{SiC}}} \tag{4.5}$$

4.1.2. Multiplication coefficient M and breakdown criteria

Avalanche breakdown occurs when the total number of electron-hole pairs generated within the depletion region approaches infinity, which also means the multiplication coefficient M goes to infinity. The following equations show the derivation of the calculations for avalanche breakdown in semiconductor pn junctions.

The variation of the electron current in the depletion region can be written as

$$\frac{dJ_n(x)}{dx} = \alpha_n(x)J_n(x) + \alpha_p(x)J_p(x) + qG(x) \tag{4.6}$$

Where q is value of the electronic charge, and G(x) is the generation rate of electron-hole pairs by absorbed photons at position x in the depletion region.

The variation of the hole current is given by

$$-\frac{dJ_p(x)}{dx} = \alpha_n(x)J_n(x) + \alpha_p(x)J_p(x) + qG(x) \tag{4.7}$$

The total current J is the sum of the electron and hole currents. Under DC conditions,

$$J = J_n(x) + J_p(x) = \text{CONSTANT} \tag{4.10}$$

Then,

$$\frac{dJ_n(x)}{dx} = [\alpha_n(x) - \alpha_p(x)]J_n(x) + \alpha_p(x)J + qG(x) \tag{4.11}$$

$$\frac{dJ_p(x)}{dx} = [\alpha_n(x) - \alpha_p(x)]J_p(x) - \alpha_p(x)J - qG(x) \tag{4.12}$$

These expressions can be solved by using the integrating factor:

$$\exp[-\int_0^x (\alpha_n - \alpha_p)dx^{'}] = \exp[-\varphi(x)] \tag{4.13}$$

And integrating from x=0 to W, the total current can be obtained:

$$J = \frac{J_p(W) + J_n(0)\exp[\varphi(W)] + q\exp[\varphi(W)]\int_0^W G(x)\exp[-\varphi(x)]dx}{1 - \int_0^W \alpha_p \exp[-\int_x^W (\alpha_n - \alpha_p)dx^{'}]dx} \tag{4.14}$$

$$J = \frac{J_p(W)\exp[-\varphi(W)] + J_n(0) + q\int_0^W G(x)\exp[-\varphi(x)]dx}{1 - \int_0^W \alpha_n \exp[-\int_0^x (\alpha_n - \alpha_p)dx^{'}]dx} \tag{4.15}$$

From (4.11) and (4.12), respectively.

The equivalence of (4.14) and (4.15) can be demonstrated by

$$-\int_0^W (\alpha_n - \alpha_p)\exp[-\int_0^x (\alpha_n - \alpha_p)dx^{'}]dx = \exp[-\int_0^W (\alpha_n - \alpha_p)dx\ ] - 1 \tag{4.16}$$

If the space-charge generation is taken as zero and hole injection at x=W and electron injection at x=0 are considered separately, the multiplication factors for electrons and holes can be obtained from (4.14) and (4.15).

$$M_n = \frac{J}{J_n(0)} = \frac{\exp[-\int_0^W (\alpha_n - \alpha_p)dx\ ]}{1 - \int_0^W \alpha_p \exp[\int_x^W (\alpha_n - \alpha_p)dx^{'}]dx} = \frac{1}{1 - \int_0^W \alpha_n \exp[-\int_0^x (\alpha_n - \alpha_p)dx^{'}]dx} \tag{4.15}$$

$$M_p = \frac{J}{J_p(W)} = \frac{1}{1 - \int_0^W \alpha_p \exp[-\int_x^W (\alpha_n - \alpha_p)dx^{'}]dx} = \frac{\exp[-\int_0^W (\alpha_n - \alpha_p)dx\ ]}{1 - \int_0^W \alpha_n \exp[-\int_0^x (\alpha_n - \alpha_p)dx^{'}]dx}$$

(4.16)

When an avalanche breakdown happens, multiplication factors M approach infinity.

Therefore, the criteria for avalanche breakdown in pn junction can be determined when the following two equations come into existence:

$$\int_0^W \alpha_n \exp[-\int_0^x (\alpha_n - \alpha_p)dx^{'}]dx = 1 \quad (4.17)$$

$$\int_0^W \alpha_p \exp[\int_x^W (\alpha_n - \alpha_p)dx^{'}]dx = 1 \quad (4.18)$$

4.1.3. Breakdown voltages and critical fields in 4H-SiC

Those effective impact ionization integral above can not be employed in 4H-SiC because the hole impact ionization coefficient α_p is much higher than the electron impact ionization coefficient α_n in the broad region of electric field [4.1].Therefore, α_n can be set as $\delta\ \alpha_p$, in which δ is considerably small constant such as 0.05. The accurate hole impact ionization coefficient as a function of temperature has been obtained experimentally in the form of $\alpha = a\exp(-b/E(x))$, and variation of impact ionization coefficients has been measured as a function of temperature for 4H-SiC by R.Raghunathan and B.J.Baliga [3.22]. Typical data are shown in Figure 4-2. The hole impact ionization coefficient varies with temperature as given below:

$$a_p = (6.3*10^6 - 1.07*10^4 T)e^{-1.79*10^7/E} \quad (4.19)$$

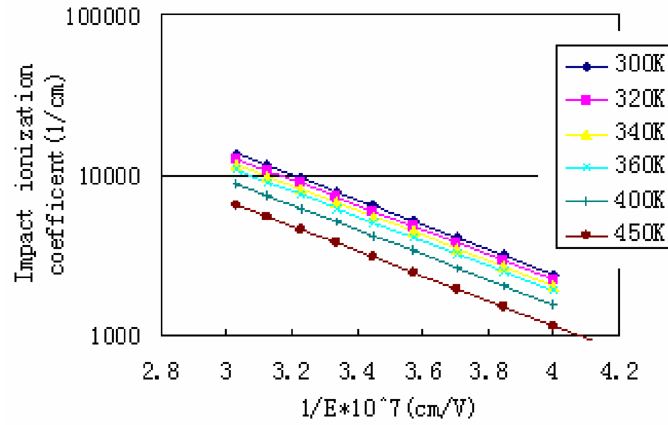

Figure 4-2. Hole impact ionization coefficients for 4H-SiC

Under room temperature, insert T=300K into (19) to obtain:

$$a_p = 0.325*10^7 e^{-1.79*10^7/E} \tag{4.20}$$

However, this form is not appropriate for ionization integral due to the exponential term including electric field. It is useful to use power law for the variation of the impact ionization coefficients with electric field similar to that suggested by Fulop [4.2] for silicon. The sixth order approximation of the impact ionization coefficient is:

$$\alpha_p = \mathrm{R}\,E^6 \tag{4.21}$$

(4.20) can be reformed by fitting into the form of (4.21):

$$\alpha_p = 1.03*10^{-35} E^6 \tag{4.22}$$

The original exponential form and the sixth order approximation are plotted as Figure 4-3, which shows the two forms fit well and the reformation is an effective way for further calculation.

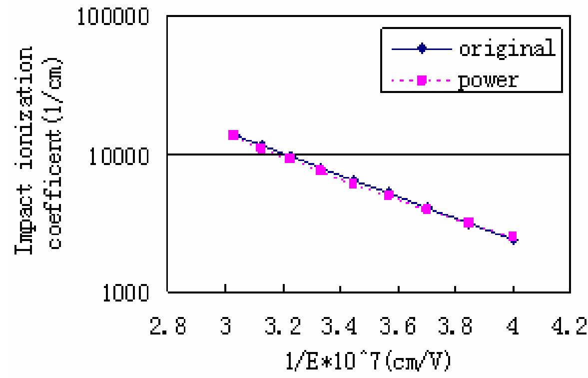

Figure 4-3. Two forms of hole impact ionization coefficients for 4H-SiC at 300K

By inserting (4.2) into (4.21), then inserting (4.21) into (4.18), the expression of critical field and depletion width can be obtained:

$$E_c = [\frac{7\ln\delta}{\delta-1}(\frac{\varepsilon_{SiC}}{q})^{-1}]^{\frac{1}{7}} R^{-\frac{1}{7}} N_D^{\frac{1}{7}} \tag{4.23}$$

$$W = [\frac{7\ln\delta}{\delta-1}(\frac{\varepsilon_{SiC}}{q})^{6}]^{\frac{1}{7}} R^{-\frac{1}{7}} N_D^{-\frac{6}{7}} \tag{4.24}$$

The breakdown voltage can also be obtained as following:

$$V_{BD} = W * E_c / 2 = [\frac{7\ln\delta}{\delta-1}(\frac{\varepsilon_{SiC}}{q})^{\frac{5}{2}}]^{\frac{2}{7}} R^{-\frac{2}{7}} N_D^{-\frac{5}{7}} \tag{4.25}$$

Where δ =0.05.

Then the critical field can be calculated and expressed by:

$$E_c = 1.69 * 10^4 N^{1/7} \tag{4.26}$$

The breakdown voltage can be expressed by:

$$V_{BD} = 7.67 * 10^{14} N^{5/7} \tag{4.27}$$

where N is the impurity concentration of the drift region.

Another theoretical dependence for hole ionization rates was proposed by Thornber [4.3]:

$$\alpha_p = \frac{eE}{E_i}\exp[-\frac{E_i}{eF\lambda(eF\lambda/3E_p+1)}] \tag{4.28}$$

For electrons, a modified form of (4.28) was used for breakdown condition derivation, which retains only the high-field asympthotics:

$$\alpha_n = \frac{eE}{E_i}\exp[-\frac{E_i}{(eE\lambda)^2/3E_p}] \tag{4.29}$$

Konstantinov *et al.* [2] provided E_i^h=7eV, E_i^e=10eV, λ_h=3.25nm, λ_e=2.99nm, E_p=0.12eV for 4H-SiC by photomultiplication measurements. By taken the data into (4.29), the hole and electron impact ionization coefficients can be expressed as followings:

$$\alpha_p = \frac{E}{7}\exp(-\frac{1}{4.2*10^{-14}E^2+0.46*10^{-7}E}) \tag{4.30}$$

$$\alpha_n = \frac{E}{10}\exp[-\frac{0.4*10^{14}}{E^2}] \tag{4.31}$$

The hole and electron impact ionization coefficients at room temperature are plotted as Figure 4-4, which shows the hole impact ionization coefficient is much higher than electron impact ionization coefficient.

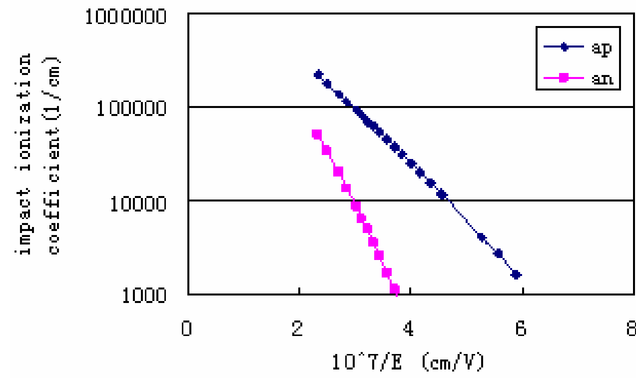

Figure 4-4. Hole and electron impact ionization coefficients for 4H-SiC at 300K

The form of (4.30) and (4.31) is not appropriate for ionization integral due to the exponential term including electric field. They can be modified into polynomial by curve fitting:

$$\alpha_p = 3*10^{-8}E^2 - 0.0917E + 70977 \tag{4.32}$$

$$\alpha_n = 2*10^{-8}E^2 - 0.0873E + 114176 \tag{4.33}$$

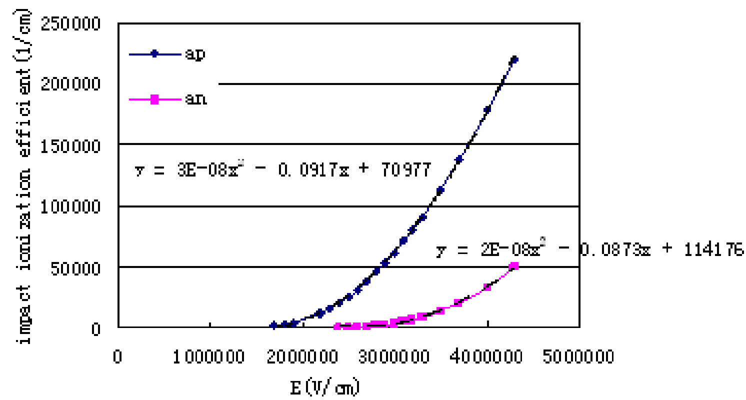

Figure 4-5.Impact ionization coefficients and their poly form for 4H-SiC at 300K

With (4.18), (4.32) and (4.33), the breakdown voltages and fields can be calculated numerically. Theoretical dependence for critical field and breakdown voltage can be

achieved through the curve fitting.

The critical field can be obtained as following expression:

$$E_c = \frac{2.49*10^6}{1.2 - 0.1335\log(\frac{N}{10^6})} \qquad (4.34)$$

The power-law approximation for breakdown voltage is as following expression, which has been plotted in Figure 4-6:

$$V_{BD} = 1976.6*(\frac{N}{10^{16}})^{-0.76} \qquad (4.35)$$

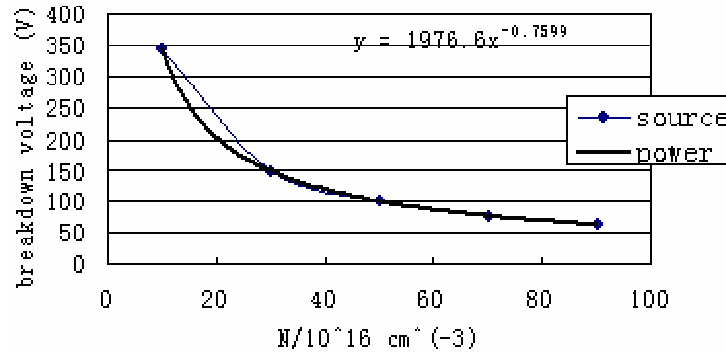

Figure 4-6. Breakdown field VS doping concentration in 4H-SiC

4.2 Challenge and consideration in simulation of reverse characteristics of SiC pn junction in MEDICI

The above calculations of the breakdown voltage, critical field, and depletion width can be used as useful tools in SiC power device field and refer only to defect free bulk material. Simulation tool MEDICI simulates the ideal device characteristics of SiC device by incorporating these calculation models for ideal devices by default. However, in real devices, avalanche breakdown may take place earlier than the defect free SiC device.

Therefore, MEDICI, which has only incorporated model for defect free material by default, can not predict the characteristics of the practical devices with defects.

The low intrinsic carrier concentration at room temperature caused by the wide bandgap raises one difficulty in the SiC device simulation in MEDICI, the reverse voltage no breakdown problem. When the simulator has to deal with the majority carrier concentration on the order of $10^{18}cm^{-3}$ and a minority carrier concentration of less than $10^{-18}cm^{-3}$, the numerical accuracy is not enough. In addition, ideal minority carrier concentrations in SiC are too low to give meaningful calculation of impact ionization rates, which will make the simulation hard to converge.

Another one is, due to the uncertainty of some parameters and the high density, the mismatches of simulation results with reported device characteristics such as reverse breakdown voltage are extremely large, taking the data extracted from [4.4] for example, as shown in Figure 1-3. This problem will be solved by the methodology discussed in the following section.

4.3 Simulation methodology of breakdown voltage of 4H-SiC pn junction diode

4.3.1 Physical analysis

The simulation can not reflect the characteristics of practical 4H-SiC pn junction diode mainly because of the high density of defects in practical 4H-SiC pn junction diode. Therefore, the physical characteristics of the main defects which influence the

performance of 4H-SiC pn junction diode should be analyzed.

The common defects in SiC epi-layers can be classified into two types: surface defects and crystal defects [4.5]. The surface defects, such as small growth pits and scratches, mainly affect the Schottky junction devices. There are mainly three types of crystal defect detrimental to pn junctions which have been identified, namely, micropipes, inclusions, and elementary screw dislocations. Figure 4-7 shows the top view and cross section of the common SiC epilayer defects that may affect the breakdown voltage.

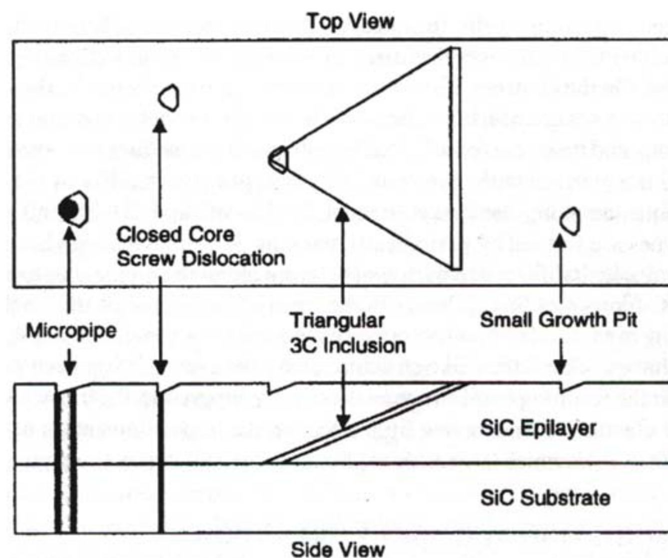

Figure 4-7. The schematic diagram of some common SiC epilayer defects[4.6]

Among these three defects, micropipes have been studied in more research activities. Micropipes are the major defect detrimental to the breakdown of SiC junction. Owing to the low stacking fault energy, SiC is also prone to inclusions of different polytypes. As has been introduced in Chapter 2, although the breakdown voltage reduced by these two

kinds of defect can be 50% or lower than the ideal bulk avalanche breakdown, their densities have been reduced to less than 1cm^{-2} and 5cm^{-2} [4.5], respectively. Hence the focus turns to the study of elementary screw dislocations.

Dislocation deserves more consideration because of its stability determined by its structure and its influence on the bulk material of 4H-SiC. Screw dislocation is very common in many processes, especially in the crystal growth, mentioned in Chapter 2. Higher annealing temperatures after implantation also cause dislocation loops. The screw step of dislocation leads to smooth deformation in the lattice along a spiral path. In describing dislocations, a very important parameter, the Burgers vector b, is used to describe the state of slip that generates a dislocation. It specifies the direction and distance by which atoms in one plane have moved from the atoms in another place. Burger vector is defined as a closure failure arising in a cycle surrounding the dislocation. A spiral ramp of a screw dislocation with the mark of the Burger vector is shown in Figure 4-8 and Figure 4-9. Elementary screw dislocations, known as close-core screw dislocations, are formed from screw dislocations with a small Burgers vector. They have closed cores in contrast to the hollow cores of micropipes.

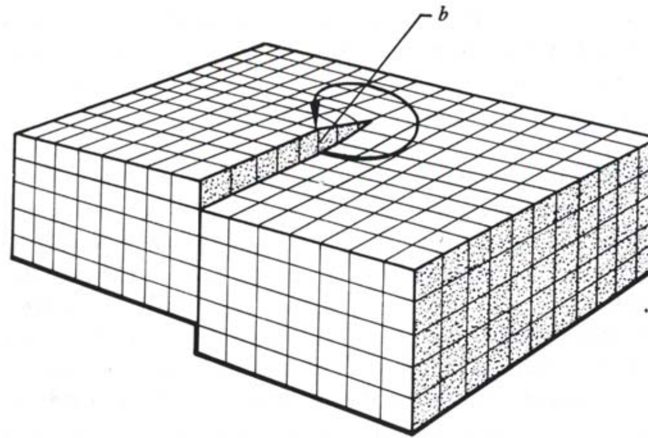

Figure 4-8. Spiral ramp of a screw dislocation with Burger vector *b* [4.7]

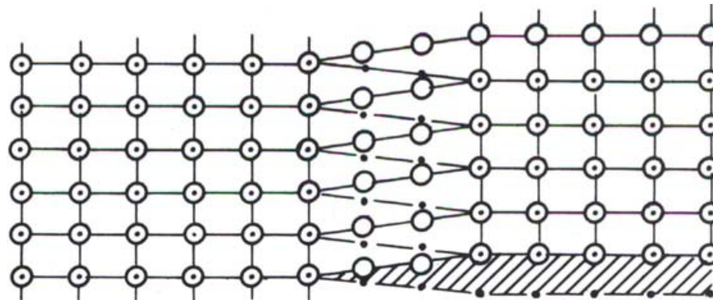

Figure 4-9. Model of ideal screw dislocation.[4.7]

Elementary screw dislocations are not as harmful as micropipes and inclusions to bulk avalanche breakdown. The breakdown voltage reduction owing to elementary screw dislocations ranges from 10% to 30% compared to the ideal breakdown voltage. However, the density of elementary screw dislocations is several orders of magnitude higher than

that of micropipes and inclusions, ranging from 10^3 cm^{-2} to $10^4 cm^{-2}$ [4.5]. This high density makes them the most detrimental defects for 4H-SiC pn junction diode.

The impact of the elementary screw dislocations on the electrical characteristics of SiC devices containing such defects is analyzed as follows. It has been reported that the variation of SiC diode reverse characteristics is determined primarily by the enhanced impact ionization process due to the dislocation defects [4.8]. The presence of dislocations leads to the creation of states within the band gap due to the crystallographic mismatch between two adjacent atoms. Charge trapping at these sites modifies the internal electric field. Since the impact ionization rates are exponentially dependent on the distribution of the electric field, such changes in the electric field under a certain reverse bias voltage can dramatically influence the device breakdown voltage and leakage current. The modified breakdown voltage due to this mechanism should depend on the energy levels and density of the states. The state levels of dislocations are reported in [4.9] to be at (E_C - 0.3 eV) and (E_V + 0.4 eV).

One other important defect subject to extensive study is deep intrinsic defects that cause semi insulating properties to SiC. Normally semi insulating properties can be obtained by introducing Vanadium. But in HTCVD process, low doped and semi-insulating material can be obtained without intentional introduction of deep impurities. The origin of the residual defects causing this is not fully understood. However, the presence of deeper defect such as the Si vacancy and the UD1 defect states has been observed using FTIR and PL spectroscopy. Samples with a dominating UD1 defect is thermally stable up to annealing temperatures of 1600 ℃.

In addition, the irradiation during ion implantation will create an intrinsic defect with associated bound excitons in the near bandgap region, which has also been subject to extensive study and can sometimes also be seen in as-grown material. These defects are temperature stable and have hole attractive potentials, which are hard to be removed during annealing.

The influence of the defect to avalanche breakdown, other than the defects discussed above, has not been identified. However, Zheng et al. [4. 8] has reported that deep traps introduced by other defects may also influence the breakdown voltage. The higher the trap density is, the lower the breakdown voltage will be.

In summary, the various defects in 4H-SiC pn junction diode can influence the breakdown voltage substantially. The main defects which are influencing the breakdown voltage of the 4H-SiC pn junction diode are the dislocations and some deep traps created by some other defects. As the trap levels created by other defect is uncertain and the trap levels created by dislocations has been known already, in the simulation work of this thesis, only the trap levels of the dislocation will be considered and incorporated.

4.3.2 Simulation methodology

To simulate the practical 4H-SiC pn junction diode, the simulations of this work take the existence of all the defects into account by using model **TRAP** in MEDICI. To analyze traps, recombination and trapping processes are analyzed at each trap energy level in

MEDICI. For recombination, the Shockley-Read-Hall (SRH) model is used. Trapping process is also modeled using SRH model. The following expression is the trap occupation function for electron traps, where f has a maximum value of 1, indicating completely filled traps:

$$f_i = \frac{\tau_{p_i} n + \tau_{n_i} p_{t_i}}{\tau_{p_i}(n + n_{t_i}) + \tau_{n_i}(p + p_{t_i})} \tag{4.36}$$

Poisson equation, normally used in the self-consistent solution of the standard device equation, is modified to include the number of electrons that are trapped.

$$\varepsilon \nabla^2 \psi = -q(p - n + N_D^+ - N_A^- - \sum_i N_{t_i} f_i) - \rho_s \tag{4.37}$$

where ψ is the intrinsic fermi potential. p and n are hole and electron concentrations, respectively. N_D^+ and N_A^- are the ionized impurity concentrations. ρ_s is a surface charge density that may be present due to fixed charge in insulating materials or charged interface states. N_{t_i} is the total number of traps for the i th energy level. N_{t_i} is calculated from the **N.TOTA**L parameter on the **TRAP** statement and is also a function of energy and position. If the trap state is specified as **CHARGED**, then the following form of the Poisson equation is used.

$$\varepsilon \nabla^2 \psi = -q(p - n + N_D^+ - N_A^- - \sum_i N_{t_i}(f_i - 1)) - \rho_s \tag{4.38}$$

Because all the defects discussed above will create traps in the bandgap, this work will incorporate these as traps in the simulation. The trap energy identified in [4.9] for dislocations, which is the main factor influencing the breakdown voltage, will be

considered and density can be adjusted by adjusting the charged trap density parameter **N.TOTAL** in **TRAP** model. Thus the simulation results are able to reflect the influence of defects on practical SiC device.

Since most of the defects occur during growth and implantation, defect density should be a function of the parameters associated with these processes. According to the physical analysis of defects above, we can assume that the trap density created by defects is related to drift layer concentration and thickness. Higher concentration of implantation will lead to a larger defect density. Thicker drift layer will increase the implantation dose, depth and energy, which will lead to a larger defect density. Moreover, the thicker the drift layer is, the longer time it is exposed to high temperature in HTCVD when fabricating the original wafer, which will also lead to larger defects density. Therefore, a linear expression for trap density (cm^{-3}) is assumed as:

$$D_{trap} = \alpha \times N + \beta \times W \qquad (4.39)$$

where N (cm^{-3}) is the drift layer concentration, and W (μm) is the thickness of drift layer. α and β should account for parameters of trap density induced by implantation. β should account for parameters of intrinsic trap density induced during growth. The value of these parameters will be empirically obtained by simulation and curve fitting.

A collection of data of reported 4H-SiC pn junction diodes [4.11-4.14] of typical design are studied. The breakdown voltage reductions of these diodes are 30% ~ 50% lower compared to theoretical prediction. The simulations of these reported 4H-SiC diodes were done by including the **TRAP** statement in MEDICI and adjusting the charged trap

density parameter **N.TOTAL** to match the reported breakdown voltage. The dislocation levels are at E_C - 0.3eV and E_V + 0.4 eV [4.9]. The influence range of one dislocation can reach a diameter of 50μm [4.10]. So in the simulation the trap model is applied for the whole region of a device.

As mentioned in the last section, ideal minority carrier concentrations in SiC are too low to give meaningful calculation of impact ionization rates. Therefore, photogeneration is added at pn junction to emulate higher carrier concentration in reverse characteristics simulation. Here we set **A1** in photogeneration model to be 10% of the doping concentration of the drift layer. Simulated breakdown voltage will not be affected when **A1** is limited to the range between $1\times10^{13}cm^{-3}$ and $1\times10^{18}cm^{-3}$. The changes of simulated breakdown voltage of diode [4.11, 4.14] with the changes of trap density and temperature are shown in Figure 4-10 and Figure 4-11 for low doping and high doping. The points in the following figures represent breakdown results of different trap density, and the lines are obtained by curve fitting to show the trend of the change.

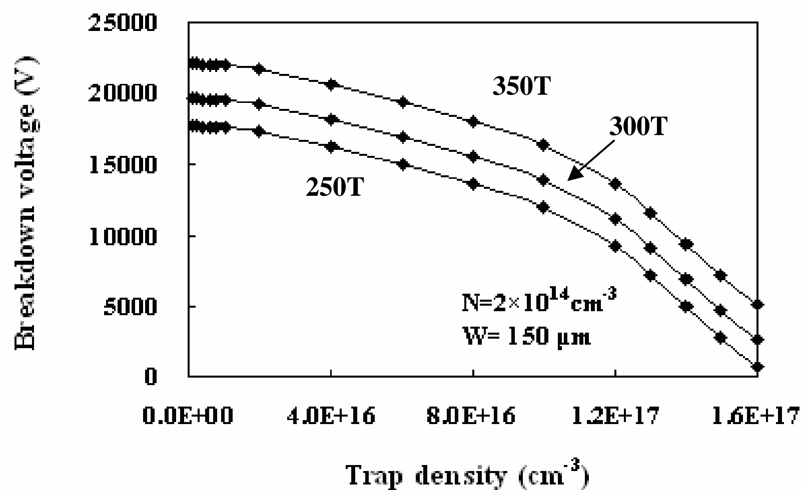

Figure 4-10. Breakdown voltage of 4H-SiC pn junction diodes [4.11] vs. Trap density.

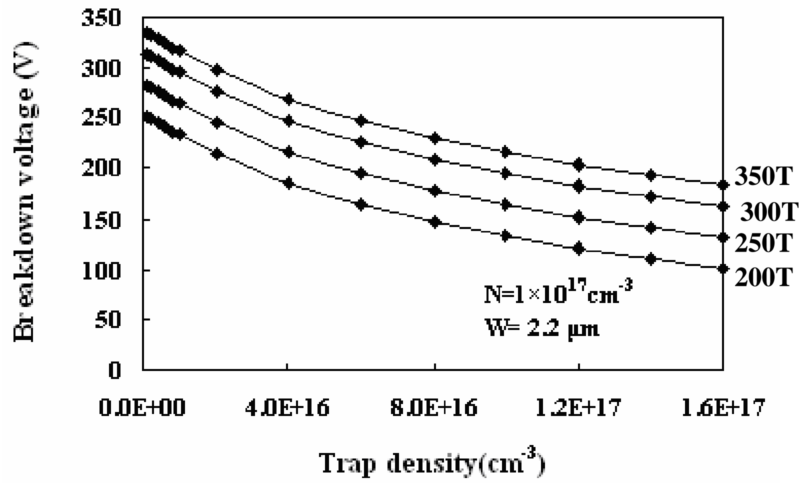

Figure 4-11. Breakdown voltage of 4H-SiC pn junction diodes [4.14] vs. Trap density.

Simulation results of trap density are summarized in the Table 4-1.

Table 4-1. Reported data of 4H-SiC pn junction diodes and simulation result with adjusted trap density

Drift-Layer Concentration (cm^{-3}) and Thickness(μm)		Reported breakdown Voltage(V)	Simulated breakdown voltage without traps (V)	Simulated breakdown voltage with traps (V)	Adjusted Trap Density by Simulation (cm^{-3})
2×10^{14}[4.11]	150	10000	19710	10011	1.258×10^{17}
4×10^{14}[4.12]	60	8300	9006.6	8299.8	0.5×10^{17}
1.6×10^{15}[4.13]	35	3600	5040.1	3598.5	0.735×10^{17}
1×10^{17}[4.14]	2.2	300	316.6	299.1	0.08×10^{17}

The data in Table 4-1 are used for curving fitting in Matlab. They can be fitted into the linear expression (4.39) for trap density very well. The unknown parameters in (4.39) can be obtained. The expression for trap density is given by

$$\mathrm{D}_{\mathrm{trap}} = 0.06675\times N + 0.89\times10^{15}\times W \quad (4.40)$$

where N (cm^{-3}) is the drift layer concentration of the 4H-SiC pn junction diodes, and W (μm) is the thickness of drift layer.

To verify the above expression, a set of new experimental results of the 4H-SiC pn junction diodes [17-20] are extracted and listed below. The simulation of these diodes with traps will show whether (4.40) can be applied to the general simulation of other 4H-SiC pn junction diodes. The trap densities calculated from (4.40) were applied to the 4H-SiC pn junction diodes reported in [17-20] in the simulation trap model. Other parameters for trap model remain the same. The simulation results of breakdown voltages are compared to reported data, as shown in Table 4-2.

Table 4-2. Verification for simulation result

n-Layer Concentration (cm^{-3}) and Thickness(μm)		Reported breakdown Voltage(V)	Trap Density (cm^{-3})	Simulated breakdown voltage without traps (V)	Simulated breakdown voltage (V)
2×10^{14}[4.15]	100	8600	14272	8.9432×10^{16}	9710.7
3×10^{15}[4.16]	35	3500	3953.9	3.1497×10^{16}	3346
9.3×10^{15}[4.17]	13	1267	1682.1	1.2245×10^{16}	1294.4
1.3×10^{17}[4.18]	2	280	270.7	1.0466×10^{16}	270.5

The breakdown voltages simulated without applying trap models are also obtained, which show large difference with the data reported. The differences between simulated breakdown voltages with trap density calculated by (4.40) and reported data are much smaller. It should be noted that the default MEDICI simulations are reasonably accurate for device with small drift layer thickness indicating marginal role played by traps as expected. This confirms that to realistically simulate the 4H-SiC pn junction diodes

nowadays, trap model should be incorporated in Medici and (4.40) can be used to set the trap density.

4.4 Simulation methodology of reverse current in 4H-SiC pn junction diode

4.4.1 Physical analysis

In SiC, the intrinsic carrier concentration at room temperature is quite low caused by the wide bandgap, shown in Figure 3-1. This causes one difficulty in the SiC device simulation in MEDICI, the reverse voltage no breakdown problem. When the simulator has to cope with the majority carrier concentration on the order of $10^{18}cm^{-3}$ and a minority carrier concentration of less than $10^{-18}cm^{-3}$, the numerical accuracy is not enough. In addition, ideal minority carrier concentrations in SiC are too low to give meaningful calculation of impact ionization rates, which will make the simulation hard to converge. One way to solve this problem is to conduct simulation by adding photogeneration at 4H-SiC pn junction to artificially increase minority carrier concentration and remove it once the avalanche condition has been achieved

4.4.2 Simulation methodology

In MEDICI, photogeneration model allows the steady-state or time-dependent injection of electrons and holes into the device. The generation rate of photogeneration depends on length, radial distance and time as in (3.34).

The time dependence represents how the photogeneration will change with time. It may

be one of the four terms, Gaussian, delta, uniform or pulse. Here, we leave it to be default uniform, for the simulation is in steady state. In this case,

$$T(t) = 1 \tag{4.42}$$

The radial dependence represents the distribution of generated carrier concentration in horizontal direction.

$$R(r) = \begin{cases} \exp[-(\frac{r}{R})^2] & R > 0 \\ 1 & R = 0 \end{cases} \tag{4.43}$$

The characteristic radial distance R of charge generation can be defined as zero, which means the generated carrier concentration does not change with the radial distance and is specially uniform.

The length dependence represents the distribution of generated carrier concentration in vertical direction as in (3.37).

Parameters **A1**, **A2**, **A3**, and **A4** in the expression can be used to describe the length dependence of the photogeneration rate. We can define carriers generated in the simulation to be of constant length dependence. In this case, parameters **A2**, **A3**, and **A4** are equal to zero. The value of parameter **Al**, which represents uniform carrier generation everywhere, can determine the carrier generation rate of photogeneration, and thus increase the carrier concentration in a device to which photogeneration is applied.

According to the study by simulation, **A1** should be high enough to overcome MEDICI

noise level and at the same time should not mask the breakdown phenomena. When **A1** is set in a range between $1\times10^{13}cm^{-3}$ and $1\times10^{18}cm^{-3}$, simulation results of breakdown voltage should not be affected by the photogeneration added.

In the simulation of the practical 4H-SiC pn junction at reverse bias here, photogeneration is added at pn junction to emulate higher carrier concentration. The change of parameter **A1** in photogenration model of MEDICI will affect the carrier concentration and thus the leakage current at reverse bias voltage. The influence of A1 to the leakage current of a 4H-SiC pn junction diode [4.19] is shown in Figure 4-12. Experimental work in [4.19, 4.20, and 4.21] reported 4H-SiC pn junction diodes with reverse current characteristics. Hence, we fit leakage current curves from [4.19, 4.20] through simulation by adjusting the **A1** parameter. The value of reverse current is rather small, which make it hard to measure the value precisely. And the value can be affected by various factors, such as dopings, defects, and fabrication techniques. Thus, we only fit the reported curves approximately with adjusted parameter **A1.**

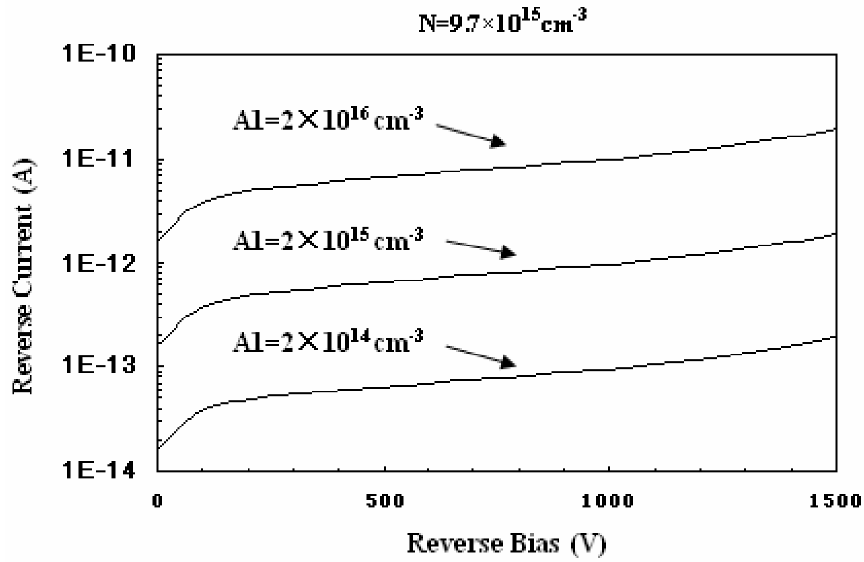

Figure 4-12. Influence of A1 to reverse current

4.4.2 Simulation result and verification

Simulated leakage current curves with adjusted **A1** to fit reported curves are shown in Figure 4-13 and Figure 4-14. The **A1** value set for diode [4.19] with drift layer concentration $9.7\times10^{15}cm^{-3}$ is 2×10^{15} cm^{-3}. The *A1* value set for diode [4.20] with drift layer concentration $3\times10^{15}cm^{-3}$ is 1×10^{14} cm^{-3}. As mentioned above, simulated breakdown voltage will keep constant when **A1** is limited in the range between $1\times10^{13}cm^{-3}$ and $1\times10^{18}cm^{-3}$. According to these data, the value of **A1** can be optimized to be about 10% of drift layer doping concentration.

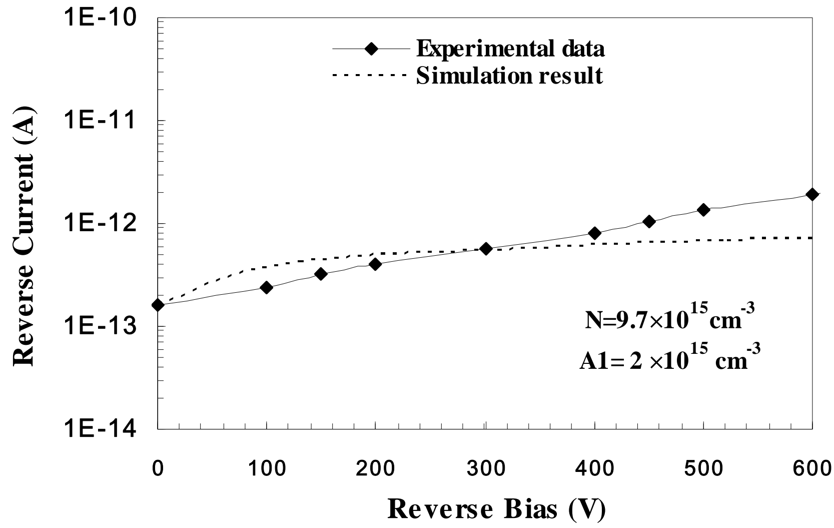

Figure 4-13: Experimental and simulated reverse current characteristics of 4H-SiC pn junction diodes [4.19].

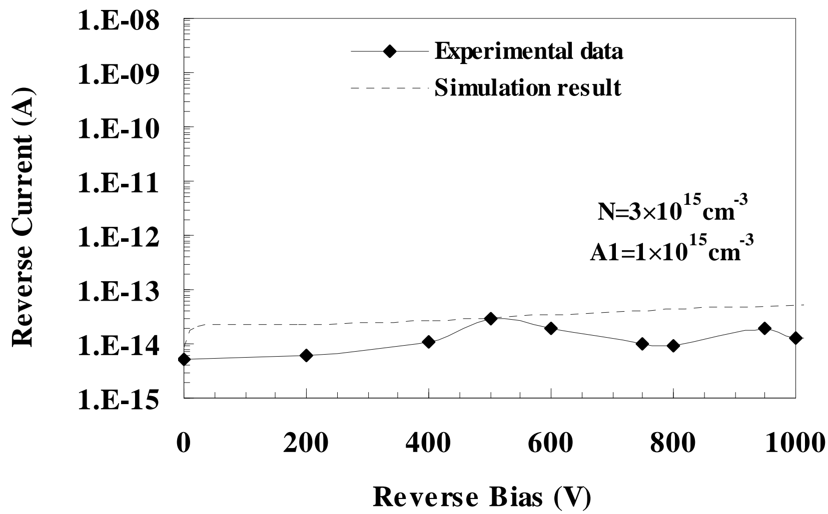

Figure 4-14: Experimental and simulated reverse current characteristics of 4H-SiC pn diodes junction [4.20].

This optimized **A1** can help to adjust reverse current depending on 4H-SiC doping concentration, substrate quality and fabrication environment. If the substrate quality, and/or fabrication environment are relatively good, a slightly lower value below 10% of doping concentration can be picked up for simulation. And vise versa.

Reported leakage current for diode reported in [4.21] with drift layer concentration $1\times10^{15}\text{cm}^{-3}$ is simulated with the optimized **A1** of $1\times10^{14}\,\text{cm}^{-3}$. Very good match of the simulated leakage current with reported experimental data as shown in Figure 4-15 verifies that the methodology is well applicable to 4H-SiC pn junction diodes.

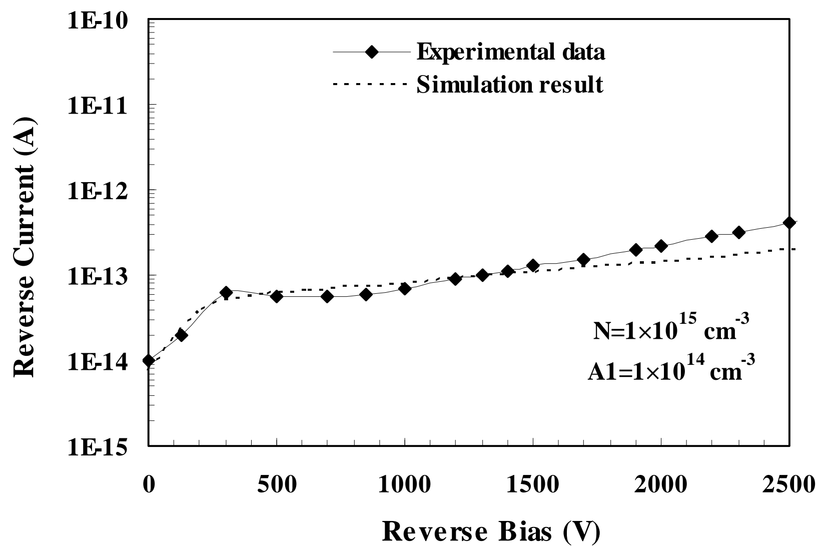

Figure 4-15: Application of the methodology to predict reversed current characteristics of a reported 4H-SiC pn junction diode [4.21].

4.5 Summary

In this chapter, the impact of the elementary screw dislocations on the reverse

characteristics of SiC devices containing such defects has been analyzed. Simulation of the reported 4H-SiC pn junction diode takes the existence of all the defects into account by using trap model in MEDICI and adjusting the charged trap density parameter **N.TOTAL** to match the reported breakdown voltage. Simulation result of trap density is summarized and analyzed by curve fitting in MATLAB. An expression of trap density (4.40) as a function of drift layer thickness and doping concentration is obtained. The leakage current curves from two experimental works have been fitted through simulation by adjusting the **A1** parameter in photogeneration model. The value of **A1** can be optimized to be about 10% of drift layer doping concentration. Simulation of other reported diodes by using the methodology match the experimental results very well, which verifies the methodology can be well applied to general simulation of 4H-SiC pn diode.

Chapter 5

Realistic Simulation of Forward Characteristics of 4H-SiC pn Junction Diode

For power devices, on-state characteristics also play an important role in power application and thus simulation of forward characteristics is useful for research in 4H-SiC device area. In this chapter, forward characteristics of 4H-SiC pn junction and relevant calculation will be introduced. Models and parameters with physical values for simulation of forward conduction characteristics of 4H-SiC pn junction diode will be presented.

5.1. Forward characteristics of 4H-SiC pn junction

Before doing the simulation, to understand the details of all the components of the forward current of 4H-SiC pn junction diode is necessary. Considering a p+/n- junction, the injection of minority carriers plays a major role in the forward characteristics of the basic pn junction. Therefore, the nature of the forward conduction current depends strongly upon the current level.

5.1.1. Recombination without injection

At the beginning of forward characteristics under low forward bias, the current is dominated by recombination within the space charge layer of the pn junction due to

the existence of deep levels. The minority carrier concentration on the P+ side can be expressed as:

$$n = \frac{n_i^2}{N}\exp(\frac{qV}{kT}) \tag{5.1}$$

Based on the Shockley-Read-Hall theory for recombination via a deep level impurity, the recombination rate can be expressed as:

$$U = \frac{np - n_i^2}{\tau \ (n + p + 2n_i)} \tag{5.2}$$

Substituting (5.1) into (5.2), the recombination rate could be

$$U = \frac{n_i}{2\tau}[\exp(\frac{qV}{2kT}) - 1] \tag{5.3}$$

Every carrier within the depletion region will participate in the conduction current creating a current flow:

$$J = \frac{qn_iW_D}{2\tau}[\exp(\frac{qV}{2kT}) - 1] \tag{5.4}$$

where W_D is the depletion width. This form of current-voltage expression is applicable at very low current level.

5.1.2. Low level injection

As the forward bias increases, the current is determined by recombination of minority carriers injected into the neutral regions. The minority carrier density injected into the neutral regions is below the majority carrier density, which refers to low level injection. In this case, the effect of majority carrier concentration can be neglected. Under steady state conditions in deal diode, assuming that there is only drift and

diffusion in forward conduction, the forward current density in pn junction diode can be calculated as:

$$J = J_N(x) + J_P(x) \tag{5.5}$$

where

$$J_N(x) = q\mu_n nE + qD_N \frac{dn}{dx} \tag{5.6}$$

$$J_P(x) = q\mu_p pE - qD_P \frac{dp}{dx} \tag{5.7}$$

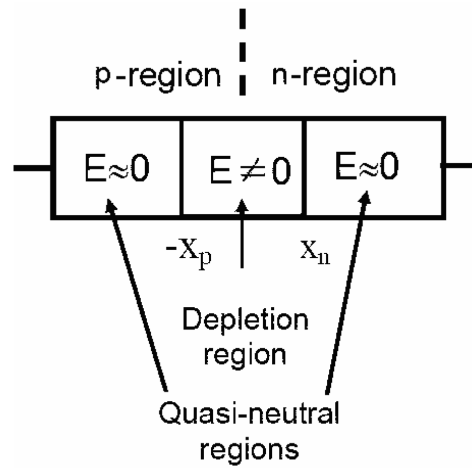

Figure 5-1 A scheme of a pn junction diode under low injection condition

As shown in Figure 5-1, the minority carrier equations for the p and n quasinetrual regions are

$$0 = D_N \frac{d^2 \Delta n_p}{dx^2} - \frac{\Delta n_p}{\tau_n} \qquad x \le -x_p \tag{5.8}$$

$$0 = D_P \frac{d^2 \Delta p_n}{dx^2} - \frac{\Delta p_n}{\tau_p} \qquad x \ge x_n \tag{5.9}$$

In low level injection,

$$E = 0 \tag{5.10}$$

$$\frac{dn_0}{dx} = \frac{dp_0}{dx} = 0 \tag{5.11}$$

From (5.10) and (5.11), current density in these two quasinetral regions can be calculated:

$$J_N(x) = qD_N \frac{d\Delta n_p}{dx^2} \qquad x \le -x_p \tag{5.12}$$

$$J_P(x) = -qD_P \frac{d\Delta p_n}{dx^2} \qquad x \ge x_n \tag{5.13}$$

According to continuity equations:

$$0 = \frac{1}{q} \times \frac{dJ_N}{dx} + \frac{\partial n}{\partial t}\Big|_{R-G} \tag{5.14}$$

$$0 = -\frac{1}{q} \times \frac{dJ_p}{dx} + \frac{\partial p}{\partial t}\Big|_{R-G} \tag{5.15}$$

In ideal diode, it can be assumed that thermal recombination and generation current is negligible. So the following can be obtained:

$$J_N(-x_p \le x \le x_n) = J_N(-x_p) \tag{5.16}$$

$$J_P(-x_p \le x \le x_n) = J_P(x_n) \tag{5.17}$$

Then, the total current density in the depletion region can be calculated as

$$J = J_N(-x_p) + J_P(x_n) \tag{5.18}$$

According to law of injection, continuity equation (5.8) and (5.9), and the boundary condition,

$$\Delta p_n(x = \infty) = 0 \tag{5.19}$$

The following can be obtained,

$$\Delta p_n(x) = A_1 \exp(\frac{-x}{L_p}) + A_2 \exp(\frac{x}{L_p}) \tag{5.20}$$

Where

$$L_p = \sqrt{D_p \tau_p} \tag{5.21}$$

$$A_1 = \Delta p_n (x = -x_p) \tag{5.22}$$

$$A_2 = 0 \tag{5.23}$$

Therefore,

$$J_p(x) = -qD_p \frac{d\Delta p_n}{dx} = q\frac{D_p n_i^2}{L_p N_D}\left[\exp\left(\frac{qV}{kT}\right) - 1\right]\exp\left(\frac{-x + x_n}{\sqrt{D_p \tau_p}}\right) \tag{5.24}$$

Similarly, it can be obtained that

$$J_n(x) = -qD_n \frac{d\Delta n_p}{dx} = q\frac{D_n n_i^2}{L_n N_A}\left[\exp\left(\frac{qV}{kT}\right) - 1\right]\exp\left(\frac{-x - x_p}{\sqrt{D_p \tau_p}}\right) \tag{5.25}$$

Thus,

$$J_p(x = x_n) = q\frac{D_p n_i^2}{L_p N_D}\left[\exp\left(\frac{qV}{kT}\right) - 1\right] \tag{5.26}$$

$$J_n(x = -x_p) = q\frac{D_n n_i^2}{L_n N_A}\left[\exp\left(\frac{qV}{kT}\right) - 1\right] \tag{5.27}$$

The whole current under low injection condition should be

$$J = q\left(\frac{D_p n_i^2}{L_p N_D} + \frac{D_n n_i^2}{L_n N_A}\right)\left[\exp\left(\frac{qV}{kT}\right) - 1\right] \tag{5.28}$$

It should be noted that the minority carrier diffusion current decrease with the distance x from the junction, while majority carrier drift current increases with the distance x from the junction. Moreover, the rate of change in forward conduction current with forward voltage bias changes from that for recombination current in the depletion region.

5.1.3. High level injection

During on-state conduction, as the current density increase, the injected carrier density increases as well and exceeds the low doping concentration of n- region, which is known as high level injection. Under steady state conditions, both minority and majority carrier concentrations adjacent to the depletion region are influenced. The majority carrier concentration must increase to maintain approximate charge neutrality in the quasineutral regions. While the low level injection current vary as $\exp(\frac{q}{kT})$ according to (5.28), detail analysis of high-level injection leads to a current varying as $\exp(\frac{q}{2kT})$ as in (5.29), where a is a constant. The current changes with the voltage under low level and high level injections are shown in Figure 5-2.

$$J = qa\left[\exp\left(\frac{qV}{2kT}\right) - 1\right] \tag{5.29}$$

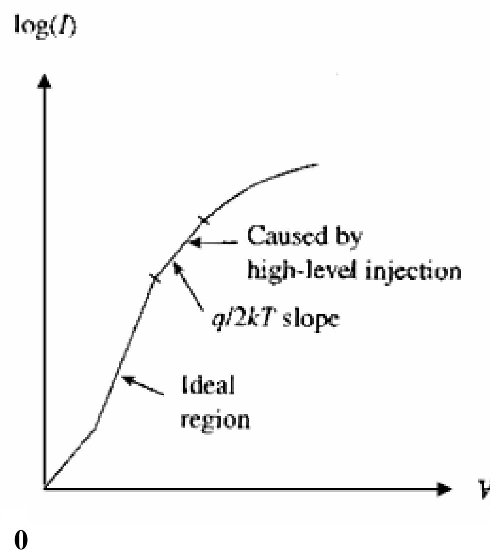

Figure 5-2. Different slop of forward characteristics caused by high level injection

5.2 Realistic simulation of forward characteristics of 4H-SiC pn junction diode

5.2.1 Simulation considerations

In MEDICI, the default model parameters can not simulate the realistic forward characteristics of 4H-SiC pn junction diode because of uncertainty of some physical value of 4H-SiC material and most of the default parameters for SiC are not for 4H polytype. In this section, physical model and parameter for simulation of forward characteristics of 4H-SiC pn junction diode are summarized, especially recombination and generation model, and the mobility model under low field and high field.

5.2.2 Simulation models and physical parameter values

To simulate forward characteristics of 4H-SiC pn junction diodes, **EG300** for 4H-SiC bandgap energy at 300K can be set as 3.26eV, and **EGALPH and EGBETA** as in (3.13) is 4.59×10^{-4} eV/K and 530 K, instead of the default value 4.73×10^{-4} eV/K and 636 K, respectively. To simulate 4H-SiC device, default values in MEDICI 1.23×10^{19} cm^{-3} and $4.58\times10^{18}cm^{-3}$ can be the values of **NC300** and **NV300** in (3.11) and (3.12) respectively. MEDICI takes the bandgap narrow effect into account as in (3.14) and (3.15), where the default values of **V0.BGN**, **N0.BGN**, and **CON.BGN** are used in 4H-SiC simulation, 9×10^{-3} V, 1.0×10^{17} cm^{-3} and 0.5, respectively. For low field mobility model, concentration and temperature dependent empirical mobility functions for silicon given by the Caughey-Thomas equation [5.1], can be selected for simulating 4H-SiC material. The parameters **MUN.MAX** and **MUP.MAX** (μ_{max}) are

the mobilities of undoped or unintentionally doped samples, which could be specified as 947.0 cm^2/Vs and 124.0 cm^2/Vs for simulation 4H-SiC device. **MUN.MIN** and **MUP.MIN** (μ_{min}) are the mobilities in highly doped material, where ionized impurity scattering is dominant, which can be specified as 0 and 15.9 cm^2/Vs. The parameters **NREFN** and **NREFP** are the doping concentrations at which the mobility is between μ_{max} and μ_{min}, which can be specified as 1.94×10^{17} cm^{-3} and 1.76×10^{19} cm^{-3}. The parameters **ALPHAN** and **ALPHAP** are the measure of how quickly the mobilities switch from μ_{max} and μ_{min}, which can be specified as 0.61 and 0.34. This analytic mobility model can be specified with the **ANALYTIC** parameter on the **MODELS** statement.

When the electric field is high enough, the carrier velocity will be no longer proportional to the field, and thus no longer can be described by a field independent mobility. Field-dependent mobility model is developed to account for carrier heating and velocity saturation effects as in (3.19) and (3.20). $\mu_{S,n}$ and $\mu_{S,p}$ are the low field mobilities which may include the scattering mechanisms. **VSATN** and **VSATP** are the saturation velocities, which can be both specified as 2.2×10^7 cm/s for 4H-SiC at 300K. And **BETAN** and **BETAP** are constants that influence how quickly the velocity rises up to saturation, which can be both specified as 1.2 for 4H-SiC at 300K. The knowledge about the high-field mobility of SiC is still limited till now. The only experimental result was published by Khan and Cooper [5.2, 5.3]. They measured the drift velocity (n-doped at about 10^{17} cm^{-3}) was measured as a function of electric field

in 4H-SiC epilayers. All experimental results are referring to a current flow perpendicular to the c-axis.

In 4H-SiC polytype, the carrier transport properties exhibit an anisotropic behavior with regard to crystallographic orientation. In MEDICI, the so-called Anisotropic Material Advanced Application Module (AM-AAM) is used to account for the anisotropy nature in 4H-SiC materials. Because the studied mention above are all done on N-type 4H-SiC, no available experimental data is available for the hole anisotropic mobility, the default values of which will be used in simulation. To simulate of 4H-SiC, **MU.N(1)**, **MU.N(2)** and **MU.N(3)** are set to be 0.83,1 and 0.83, respectively.

In forward characteristics, generation and recombination processes are modeled within the quasi-static approximation according to various physical mechanisms. All the models evaluate the recombination rate. When the overall rates are positive, they refer to recombination, and when they are negative, they refer to generation. The characteristics of each generation-recombination center vary with different process technology. Therefore, there are several quantities like the effective electron and hole lifetimes, which come up with one effective single-level SRH rate as in (3.24), where n_{ie} is the effective intrinsic concentration. τ_n and τ_p are the electron and hole lifetimes, which may be concentration dependent as in (3.26) and (3.27). For simulation of 4H-SiC, the default values for Si are used. **TAUN0** and **TAUP0** are both 10^{-7}s. **NSRHN** and **NSRHP** are both 5×10^{16} cm^{-3}.

5.2.3. Simulation result and discussion

With the physical data summarized above, simulation of the forward characteristics of reported 4H-SiC pn junction diodes [5.4], [5.5]are done. The measured experimental characteristics and simulation results are shown as Figure 5-3 and Figure 5-4, respectively.

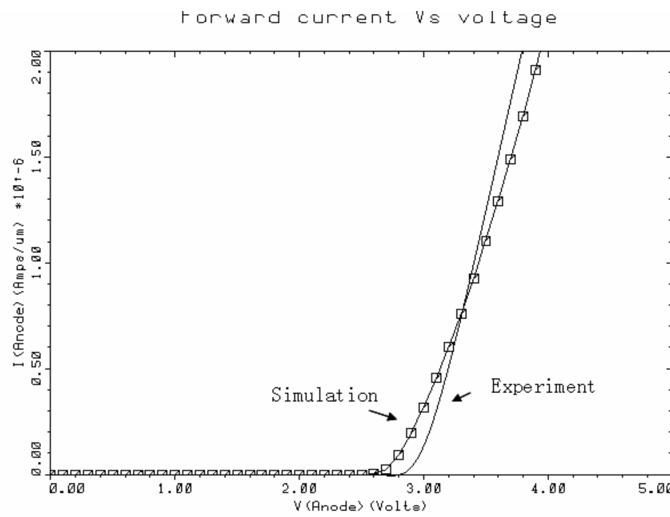

Figure 5-3. Reported forward characteristics [5.4] and Simulation result

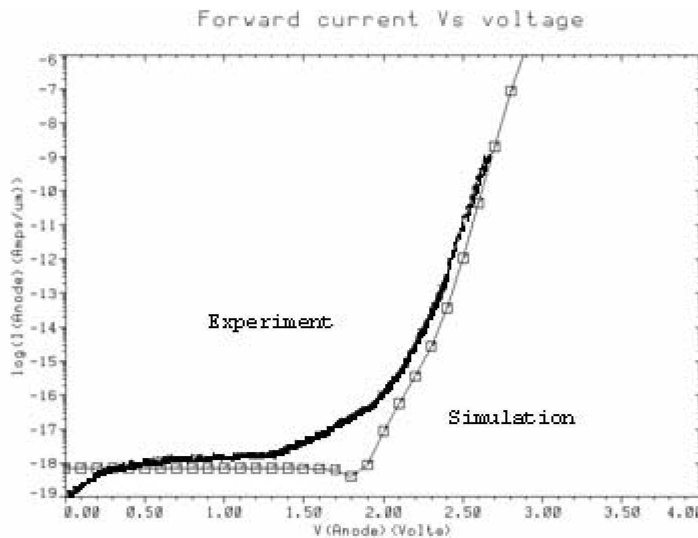

Figure 5-4. Reported forward characteristics [5.5] and Simulation result

As shown in the above Figures, the simulated result can reflect the forward

characteristics of the 4H-SiC pn junction diodes. As mentioned in last chapter, in real 4H-SiC pn junction diodes, there are various defects. Simulations with trap model incorporated have also been done for 4H-SiC pn junction diodes [5.4], [5.5], shown in Figure 5-5 and Figure 5-6.

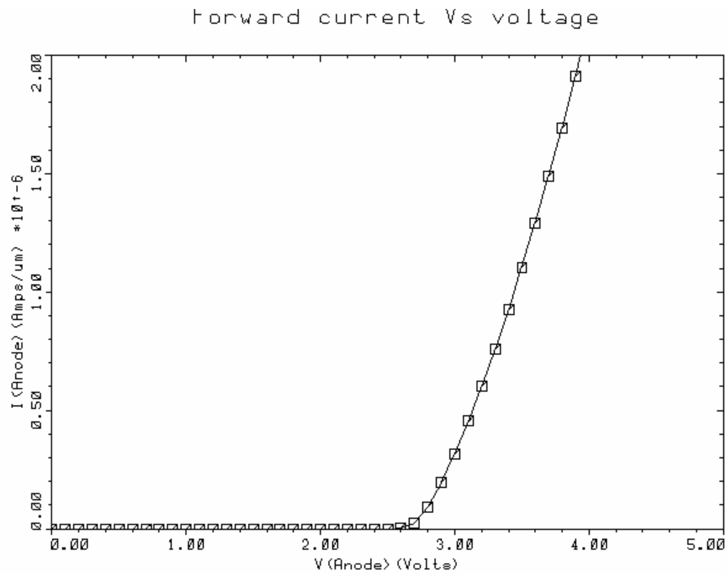

Figure 5-5. Result of forward characteristics simulation with defects of 4H-SiC pn junction diode reported in [5.4]

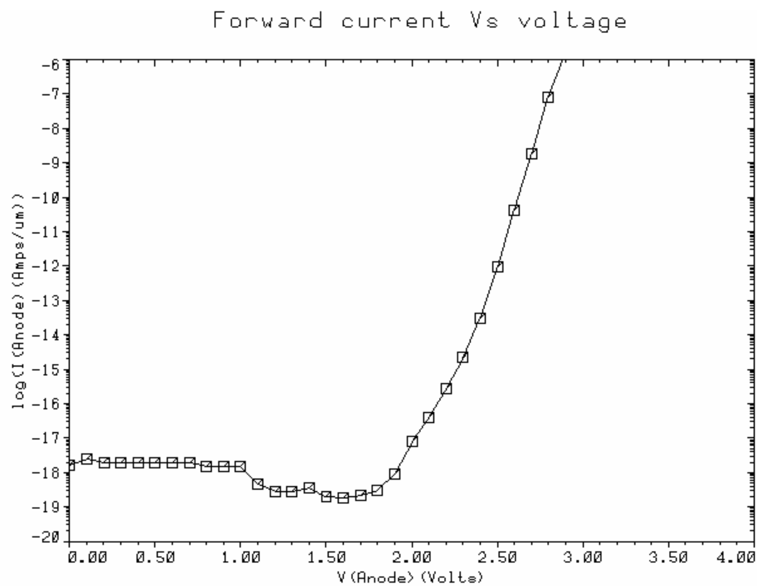

Figure 5-6. Result of forward characteristics simulation with defects of 4H-SiC pn junction diode reported in [5.5]

It can be seen that the defect levels have little influence on the forward conduction current. The simulation can save time 1-2 minutes, 25-50% of whole simulation time. Therefore, to simulate the forward characteristics of realistic 4H-SiC pn junction diodes, simulation can be done in MEDICI without incorporating TRAP model, which is needed in simulating the reverse characteristics of realistic 4H-SiC pn junction diodes. The influence of the parameters to the forward current is also simulated as following figures.

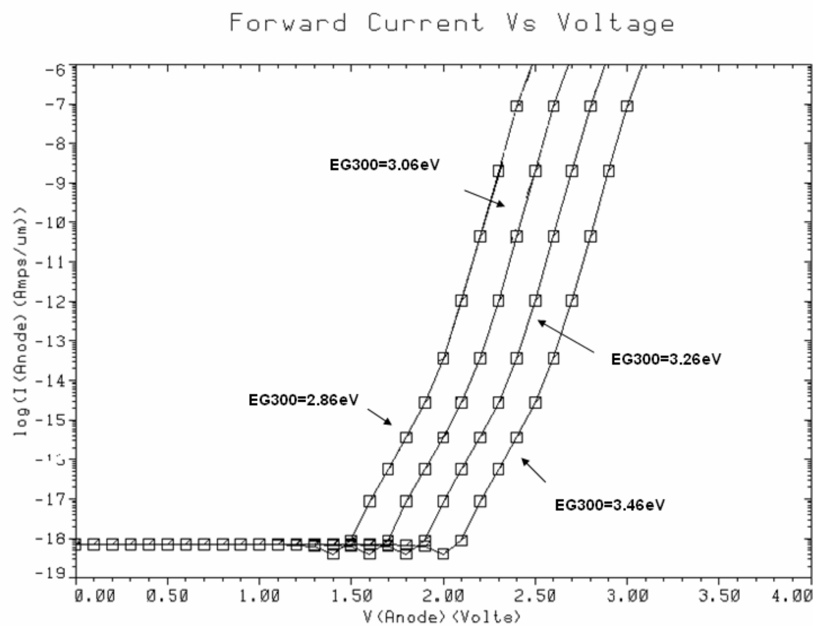

Figure 5-7. Influence of bandgap energy to the forward current reported in [5.5]

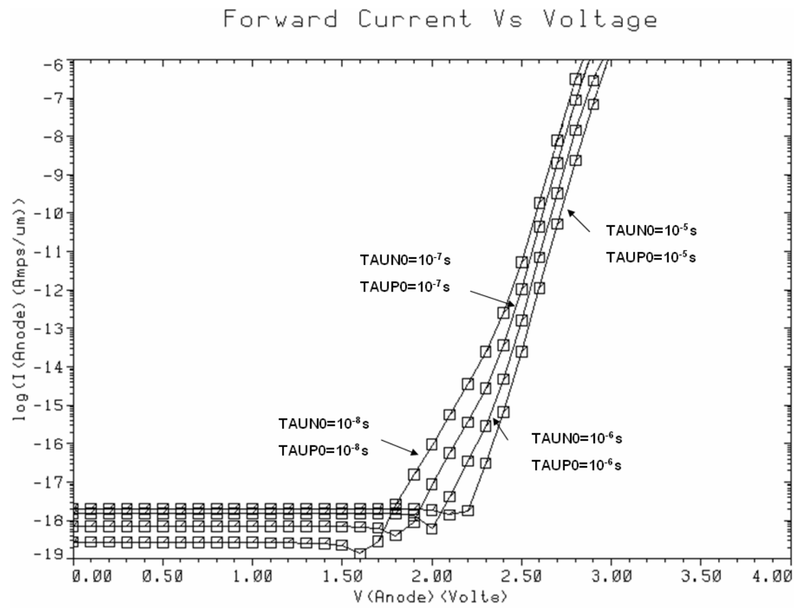

Figure 5-8. Influence of lifetime to the forward current reported in [5.5]

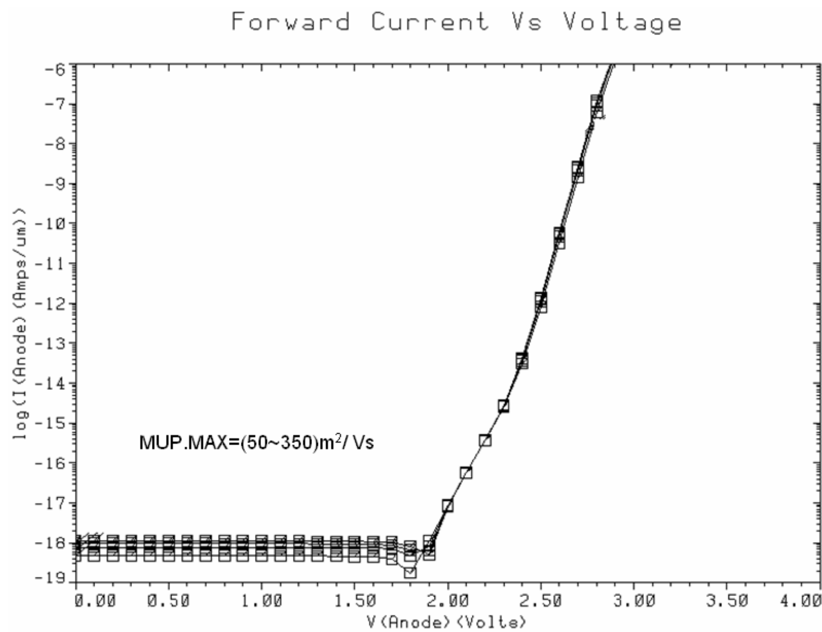

Figure 5-9.Influence of hole mobility to the forward current reported in [5.5]

Other parameters show no influence or slightly influence to the forward current. Therefore, to simulate the forward characteristics of realistic 4H-SiC pn junction diodes can be performed in MEDICI by specified the parameters with material physical value and without incorporating TRAP model.

5.3. Summary

In this chapter, forward characteristics of 4H-SiC pn junction and relevant calculation have been introduced. Models and parameters with physical values for simulation of forward conduction characteristics of 4H-SiC pn junction diode are summarized. Two reported 4H-SiC pn junction diodes are simulated by specifying the physical material parameters values. From the simulation results, it can be seen that the defect levels have little influence on the forward conduction current. Therefore, to simulate the forward characteristics of realistic 4H-SiC pn junction diodes, simulation can be done in MEDICI by specified the parameters with material physical value and without incorporating TRAP model.

Chapter 6

Conclusion

This thesis has sought to make contributions towards improvement of simulation of SiC pn junctions. A reasonably accurate and predictive methodology to simulate the forward and reverse characteristics of 4H-SiC pn junction diodes with varying doping concentration and junction depth has been developed and presented in this thesis.

The superior material properties of SiC make SiC a very promising wide band material. Due to the uncertainty of some parameters and high density of defects, the disagreement of simulation results with reported device characteristics. These are the motivation for this work. The main process techniques for SiC pn junction diode is studied, such as bulk and epitaxial growth, ion implantation and annealing process, which cause the disagreements of simulation results with reported device characteristics. Models of 2D numerical device modeling tool MEDICI are introduced for 4H-SiC device simulation. Material parameters of 4H-SiC for these models are extracted.

In chapter 4 and 5, a reasonably accurate and predictive methodology to simulate the forward and reverse characteristics of 4H-SiC pn junction diodes with varying doping concentration and junction depth is developed. Impact ionization process, along with their calculation are presented. The impact of the elementary screw dislocations on the reverse characteristics of SiC devices has been analyzed. To take the defects influence

into account in simulation, the trap density created by defects is assumed to be a function of drift layer concentration and thickness. The simulations of reported 4H-SiC diodes were done by including the **TRAP** statement in MEDICI and adjusting the charged trap density parameter **N.TOTAL** to match the reported breakdown voltage. Simulation result of trap density is summarized and analyzed by curve fitting in MATLAB. An expression of trap density (4.40) as a function of drift layer thickness and doping concentration is obtained. To verify the above expression, the trap densities calculated from (4.40) were applied to the 4H-SiC pn junction diodes reported in other literatures for simulation. The good result confirms that to realistically simulate the 4H-SiC pn junction diodes nowadays, trap model should be incorporated in Medici and (4.40) can be used to set the trap density.

To solve the reverse no breakdown problem and to improve the simulation of reverse current of practical 4H-SiC pn junction, photogeneration model is incorporated in MEDICI. According to the study by simulation, **A1** should be high enough to overcome MEDICI noise level and at the same time should not mask the breakdown phenomena. When **A1** is set in a range between $1\times10^{13}cm^{-3}$ and $1\times10^{18}cm^{-3}$, simulation results of breakdown voltage should not be affected by the photogeneration added. The leakage current curves from two experimental works have been fitted through simulation by adjusting the **A1** parameter. The **A1** value set for diode with drift layer concentration $9.7\times10^{15}cm^{-3}$ is 2×10^{15} cm^{-3}. The *A1* value set for diode with drift layer concentration $3\times10^{15}cm^{-3}$ is 1×10^{14} cm^{-3}. According to these data, the value of **A1** can be optimized to be about 10% of drift layer doping concentration. Very good match of the simulated

leakage current with another reported experimental data verifies that the methodology is well applicable to 4H-SiC pn junction diodes. This optimized **A1** can help to adjust reverse current depending on 4H-SiC doping concentration, substrate quality and fabrication environment.

Forward characteristics of 4H-SiC pn junction and relevant calculation have been introduced. Models and parameters with physical values for simulation of forward conduction characteristics of 4H-SiC pn junction diode are summarized. Two reported 4H-SiC pn junction diodes are simulated by specifying the physical material parameters values. From the simulation results, it can be seen that the defect levels have little influence on the forward conduction current. Therefore, to simulate the forward characteristics of realistic 4H-SiC pn junction diodes, simulation can be done in MEDICI by specified the parameters with material physical value and without incorporating TRAP model.

More considerations could be studied in future as followings.

a) The physical mechanism of producing the defects in fabrication process has not been studied in depth. Further study could be done on this topic and incorporate this mechanisms into the simulation for its further improvements.
b) The methodology is obtained after the problem is simplified, because the types of defect in SiC are various and the mechanisms of influencing the performance of the device caused by defect are complex to quantify. More factors will be considered in future improvement of the simulation methodology.

References

[1.1] H. M. Hobgood, D. L. Barrett, J. P. McHugh, R. C. Clarke, S. Sriram, A. A. Burk, J. Greggi, C. D. Brandt, R. H. Hopkins, and W. J. Choyke, “*Large diameter 6H-SiC for microwave device applications*”, Journal of Crystal Growth, Volume 137, Issues 1-2, pp.181-186, March 1994.

[1.2] Z.C.Feng and J.H.Zhao, Silicon Carbide Materials, Processing, and Devices, New York, London: Taylor & Francis Books , 2004

[1.3] H. Jagodzinski and H. Arnold, “*The crystal structures of silicon carbide*”, in Silicon Carbide, A High Temp. Semiconductor, J. R. O’Connor and J. Smiltens, Eds. New York: Pergamon Press Inc., 1960.

[1.4] W. J. Schaffer, G. H. Negley, K. G. Irvine, and J. W. Palmour, “*Conductivity anisotrophy in epitaxial 6H and 4H SiC*”, Mat. Res. Soc. Symp. Proc., vol. 339, Diamond, SiC, and Nitride Wide-Bandgap Semiconductors, Eds. Pittsburgh, PA: Materials Research Society, pp.595-598, 1994.

[1.5] P. G. Neudeck, D. J. Larkin, J. E. Starr, J. A. Powell, C. S. Salupo, and L. G. Matus, “*Electrical properties of epitaxial 3C- and 6H-SiC p-n junction diodes produced sideby- side on 6H-SiC wafers*”, IEEE Trans. Elect. Dev., Volume 41, Issue 4, pp.567-574, April 1994.

[1.6] Y. Sugawara, D. Takayama, K. Asano, R. Singh, J. Palmaour, and T. Hayashi, "*12-19 KV 4H-SiC p-i-n Diodes with Low Power Loss*", in Proceedings of the 13th International Symposium on Power Semiconductor Devices and ICs, ISPSD'01, pp. 27-30, 2001.

[1.7] J. Tan, J. A. Cooper, Jr., and M. R. Melloch, "*High-Voltage Accumulation-Layer UMOSFET's in 4H-SiC*", Electron Device Letters, IEEE, Volume 19, Issue 12, pp.487–489, December 1998.

[1.8] S.H. Ryu, A. Agarwal, R. Singh, and J. Palmour, "*1800 V NPN Bipolar Junction Transistors in 4H-SiC*", IEEE Electron Device Lett., Volume 22, Issue 3, pp.124-126, March 2001.

[1.9] S.H. Ryu, A. Agarwal, R. Singh, and J. Palmour, "*3100 V, Asymmetrical, Gate Turn-Off (GTO) Thyristors in 4H-SiC*", IEEE Electron Device Lett., Volume 22, Issue 3, pp.127-129, 2001.

[1.10] C. E. Weitzel, J. W. Palamour, C. H. Carter, and K. J. Nordquist, "*4H-SiC*

MESFET with 2.8 W/mm Power Density at 1.8 GHz", IEEE Electron Devices Letters, Volume 15, Issue 10, pp.406-408, October 1994.

[1.11] Purdue University, USA. http://www.ecn.purdue.edu/WBG/.

[1.12] H. M. McGloothlin, D. T. Morisette, J. A. Cooper, Jr., and M. R. Melloch, "*4 KV Silicon Crabide Schottky Diodes for High-Frequency Switching Applications*", IEEE Device Research Conference Digest, pp.42-43, 1999.

[1.13] J. B. Fedison, N. Ramungul, T. P. Chow, M. Ghezzo, and J. W. Kretchmer, "*Electrical Characteristics of 4.5 kV Implanted Anode 4H-SiC PiN Junction Rectifiers*", IEEE Electron Device Lett., vol. 22, no. 3, pp.130-132, 2001.

[1.14] P. Dahlquist, J. O. Svedberg, C. M. Zetterling, M. Ostling, B. Breitholtz, and H. Lendenmann, "*Static and Dynamic Characteristics of 4H-SiC JFETs Designed for Different Blocking Categories*", Materials Science Forum, vol. 338-342, pp.1179-1182, 2000.

[1.15] A. Hefner Jr., D. Berning, J. S. Lai, C. Liu, and R. Singh, "*Silicon Carbide Merged PiN Schottky Diode Switching Characteristics and Evaluation for Power Supply Applications*", Conference Record of the 2000 IEEE Industry Applications Conference, vol. 5, pp. 2948-2954, 2000.

[1.16] SiCED Electronics Development, Geramny. http://www.siced.de/.

[1.17] S.H. Ryu, A. Agarwal, J. Richmond, J. Palmour, N. Saks, and J. Williams, "*10A, 2.4kV Power DMOSFETs in 4H-SiC*", IEEE Trans. Electron Devices, vol. 23, no. 6, pp.321-323, 2002.

[1.18] K. Asano, Y. Sugawara, S. Ryu, R. Singh, J. Palmaour, T. Hayashi, and D. Takayama, "*5.5 kV Normally-Off Low Ron 4H-SiC SEJFET*", in Proceedings of the 13th International Symposium on Power Semiconductor Devices and ICs, ISPSD'01, pp. 23-26, 2001.

[1.19] Y. Tang, J. B. Fedison, and T. P. Chow, "*High-Voltage Implanted-Emitter 4H-SiC BJTs*", IEEE Electron Device Lett., vol. 23, no. 1, pp.16-18, 1999.

[1.20] Medici User’s Manual, Fremont, CA: Synopsys, Inc., 2005.

[1.21] A.K.Agarwal, S.Seshadri, M.MacMilan, S.S.Mani, J.Casdy, P.Sanger, and P.Shah, “*4H-SiC p-n diodes and gate turnoff thyristors for high-power, high-temperature applications*”, Solid-State Electronics, vol.44, pp.303-308, February 2000.

[1.22] M. Ruff, H. Mitlehner, and R. Helbig, "*SiC: Physics and numerical simulation*", IEEE Trans. Elect. Dev., vol. 41, pp.1040-1046, 1994.

[2.1] Z.C.Feng and J.H.Zhao, Silicon Carbide Materials, Processing, and Devices, New York, London: Taylor & Francis Books , 2004.

[2.2] E. G. Acheson, "*Production of Artificial Crystalline Carbonaceous Materials*", United States Patent 492,767 (28.02.93), 1893.

[2.3] J. A. Lely, "*Darstellung von Einkristallen von Silicium Carbid und Beherrschung von Art und Menge der eingebauten Verunreinigungen*", Berichte der Deutschen Keramischen Gesellschaft, vol. 32, pp. 229-236, 1955.

[2.4] Y. M. Tairov and V. F. Tsvetkov, "*General Principles of Growing Large-Size Single Crystals of Various Silicon Carbide Polytypes*", J.Cryst.Growth, vol. 52, no. 1, pp. 146-150, 1981.

[2.5] Cree, "*Silicon Carbide: Physical & Electronic Properties*." http://www.cree.com/Products/sic_index.asp.

[2.6] W. J. Choyke, H. Matsunami, and G. Pensl, A Review of Fundamental Questions and Applications to Current Device Technology. Wiley-VCH Verlag, 1997.

[2.7] Linköpings University, Department of Physics and Measurement Technology, Sweden,http://www.ifm.liu.se/matephys/AAnew/research/sicpart/kordina2.htm.

[2.8] P. G. Neudeck, "*SiC Technology*", in The VLSI Handbook, The Electrical Engineering Handbook Series, W.-K. Chen, Ed. Boca Raton, Florida: CRC Press and IEEE Press, pp. 6.1-6.24, 2000.

[2.9] O.Kordina, C. Hallin, A. Henry, J. P. Bergman, I. Ivanov, A. Ellison, N. T. Son, and E. Janzen, "*Growth of SiC by 'Hot-Wall' CVD and HTCVD*", Phys. stat. sol. (b), vol. 202, no. 1, pp. 321-334, 1997.

[2.10] Cree, "*Silicon Carbide: Physical & Electronic Properties*." http://www.cree.com/Products/sic_index.asp.

[2.11] St.G.Muller, R.C.Glass, and H.M.Hobgood, et al., "Progress in the industrial production of SiC substrates for semiconductor devices", Material Science Engineering. B, vol. 80, Issues 1-3, pp.327-331, 2001.

[2.12] K.A.Jones, K. Xie, D. W. Eckart, M. C. Wood, V. Talyansky and R. D. Vispute,

et al., "*AlN as an Encapsulate for Annealing SiC*", J.Appl. Phys., Vol.83, No.12, pp.8010-8015, June 1998.

[3.1] S. G. Sridhara, S. Bai, O. Shigiltchoff, R. P. Devaty, and W. J. Choyke, "*Absorption bands associated with conduction bands and impurity states in 4H and 6H SiC*", in Mat. Sci. Forum, vols. 338-342, pp. 551-554, 1999.

[3.2] I. G. Ivanov, U. Lindefelt, A. Henry, O. Kordina, C. Hallin, M. Aroyo, T. Egilsson, and E. Janzen, "*Phonon replicas at the M-point in 4H-SiC: A theoretical and experimental study*", Phys. Rev. B, vol. 58, pp.13634-13647, 1998.

[3.3] Handoko Linewih, Design and Application of SiC power MOSFET, PhD thesis, Engineering and information Technology, Giffith University.

[3.4] S. Selberherr, Analysis and Simulation of Semiconductor Devices, Wein: Springer-Verlag, 1984.

[3.5] J. W. Slotboom, "*The pn Product in Silicon*", Solid-State Electronics, vol.20, pp.279-283, 1977.

[3.6] S. Nishino, H. Suhara, H. Ono, and H. Matsunami, "*Epitaxial growth and electric characteristics of cubic SiC on silicon*", J. Appl. Phys., vol. 61, pp. 4889-4893, 1981.

[3.7] T. Tachibana, H. S. Kong, Y. C. Wang, and R. F. Davis, "*Hall measurements as a function of temperature on monocrystalline SiC thin films*", J. Appl. Phys., vol. 67, pp.6375-6381, 1990.

[3.8] C. T. Sah, T. H. Ning, and L. L. Tschopp, "*The scattering of electrons by surface oxide charges and lattice vibrations at the silicon-silicon dioxide interface*", Surf. Sci., vol. 32, pp. 561-575, 1972.

[3.9] Y. C. Cheng and E. A. Sullivan, "*Relative importance of phonon scattering to carrier mobility in Si surface layer at room temperature*", J. Appl. Phys., vol. 44, pp.3619-3625, 1973.

[3.10] D. M. Caughey and R. E. Thomas, "*Carrier Mobilities in Silicon Empirically Related to Doping and Field*", Proc. IEEE, Vol. 55, pp. 2192-2193, 1967.

[3.11] A. Schenk, Advanced Physical Models for Silicon Device Simulation. Springer, 1998.

[3.12] I. A. Khan and J. A. Cooper, Jr., "*Measurement of High-Field Electron*

Transport in Silicon Carbide", IEEE Trans. Electron Devices, vol. 47, no. 2, pp. 269-273, 2000.

[3.13] I. A. Khan and J. A. Cooper, Jr., "*Measurement of High Field Electron Transport in Silicon Carbide*", Materials Science Forum, vol. 264-268, pp. 509-512, 1998.

[3.14] M. Schadt, G. Pensl, R. P. Devaty, W. J. Choyke, R. Stein, and D. Stephany, "*Anisotropy of the electron Hall mobility in 4H, 6H, and 15R silicon carbide*", Appl. Phys. Lett., vol. 65, pp. 3120-3124, 1994.

[3.15] H. –E. Nilsson, U. Sannemo, and C. S. Petersson, "*Monte Carlo simulation of electron transport in 4H-SiC using a two-band model with multiple minima*", J. Appl. Phys., vol.80, pp. 3365-3369, 1996.

[3.16] R. Mickevicius, and J. H. Zhao, "*Monte Carlo study of electron transport in SiC*", J.Appl. Phys., vol. 83, pp.3161-3167, 1998.

[3.17] W. Shockley and W. T. Read, Jr., "*Statistics of the Recombinations of Holes and Electrons*", Phys. Rev., vol. 87, no. 5, pp. 835-842, 1952.

[3.18] M. Lundstrom, Fundamentals of Carrier Transport. Cambrideg Unversity Press, 2nd ed., 2000.

[3.19] J. W. Slotboom, "*The pn product in silicon*", Solid-State Elect., vol. 20, pp. 279-283, 1977.

[3.20] M. Ruff, H. Mitlehner, and R. Helbig, "*SiC: Physics and numerical simulation*", IEEE Trans. Elect. Dev., vol. 41, pp. 1040-1054, 1994.

[3.21] J. W. Palmour and L. A. Lipkin, Cree, Inc. "*High temperature power devices in silicon carbide*", in Trans. 2nd Intl. High Temp. Elect. Conf., Charlotte, June 5-10, pp. 3-6, 1994.

[3.22] R. Raghunathan and B. J. Baliga, "*Temperature dependence of hole impact ionization coefficients in 4H and 6H-SiC*", Solid-State Elect., vol. 43, pp.199-211, 1999.

[4.1] A.O.Konstantinov, Q.Wahab, N.Nordell and U.Lindefelt, "*Study of Avalanche Breakdown and Impact Ionization in 4H Silicon Carbide*", Journal of Electronic Material, vol.27 pp. 335-341,1997.

[4.2] Fulop. W, "Calculation of avalanche breakdown voltages of silicon p-n junctions", Solid-state Electronics, vol. 10, pp.39-43, 1967.

[4.3] K.K.Thornber, "Applications of scaling to problems in high-field electronic transport", J.Appl.Phys., Vol 52, pp279-290, 1981.

[4.4] A.K.Agarwal, S.Seshadri, M.MacMilan, S.S.Mani, J.Casdy, P.Sanger, and P.Shah, "*4H-SiC p-n diodes and gate turnoff thyristors for high-power, high-temperature applications*", Solid-State Electronics, vol.44, pp.303-308, February 2000.

[4.5] Z.C.Feng and J.H.Zhao, Silicon Carbide Materials, Processing, and Devices, New York, London: Taylor & Francis Books, Chap.6-7, 2004.

[4.6] Z.C.Feng and J.H.Zhao, Silicon Carbide Materials, Processing, and Devices, New York, London: Taylor & Francis Books, Chap.7, 2004.

[4.7] H.F.Matare, Defect Electronics in Semiconductors, John Wiley & Sons, Inc.,USA, 1971.

[4.8] L.Zheng, R.P.Joshi, and C.Fazi, "*Dislocation defect based model analysis for the pre-breakdown reverse characteristics of 4H-SiC p+n diodes*", Journal of Applied Physics, vol.85, pp.7935-7938, June 1999.

[4.9] A.T.Blumenau, R.Jones, S.Öberg, P.R.Briddon, and T.Frauenheim, "*Basal plane partial dislocations in silicon carbide*", Physica B: Condensed Matter, vol340-342, pp.160-164, December 2003.

[4.10] H.F.Mataré, Defect Electronics in Semiconductors, New York: John Wiley & Sons, Inc, Chap. 14, 1971.

[4.11] S.E.Saddow, et. al., "*High temperature electrical activation in 4H and 6H-SiC in a Silane ambient to reduce step bunching*", Material Science Forum, vols.338-342, pp.901-904, 2000.

[4.12] K.Vassilevski, K.Zekentes, G.Constantinidis, and A.Strel'chuk, "*Fabrication and electrical characterization of 4H-SiC p+-n-n+ diodes with low differential resistance*", Solid-State Electronics, vol.44, pp.1173-1177, July 2000.

[4.13] D.Peters, R.Elpelt, R.Schörner, K.O.Dohnke, P.Friedrichs, and D.Stephani, "*Large area, avalanche-stable 4H-SiC PiN diodes with VBR>4.5kV*", Material Science Forum, vols.483-485, pp.977-980, 2005.

[4.14] M.K.Das, J.J.Sumakeris, M.J.Paisley, and A.Powell, "*High power 4H-SiC PiN diodes with minimal forward voltage drift*", Material Science Forum, vols.457-460, pp.1105-1108, 2004.

[4.15] W.Bahng, G.H.Song, H.W.Kim, K.S.Seo, and N.K.Kim, "*Fabrication and characterization of 4H-SiC pn diode with field limiting ring*", Material Science Forum, vols.457-460, pp.1013-1016, 2004.

[4.16] R.Singh, J.A.Cooper, M.R.Melloch, T.P.Chow, and J.W.Palmour, "*SiC power Schottky and PiN diodes*", IEEE Transactions on Electron Devices, vol.49, pp.665-672, April 2002.

[4.17] D.Åberg, A.Hallén, J.Österman, U.Zimmermann, B.G.Svensson, "*The deep boron level in high voltage PiN diodes*", Material Science Forum, vols.389-393, pp.1309-1312, 2002.

[4.18] H.Sugimoto, S.Kinouchi, Y.Tarui, M.Imaizumi, K.Ohtsuka, T.Takami, and T.Ozeki, "*Planar p-n diodes fabricated by MeV-energy and high-temperature selective implantation of aluminum to 4H-SiC*", Material Science Forum, vols.353-356, pp.731-734, 2001.

[4.19] Y.Sugawara, D.Takayama, K.Asano, R.Singh, J.Palmour, and T.Hayashi, "*12-19kV 4H-SiC pin diodes with low power loss*", in Proc. IEEE International Symposium on Power Semiconductor Devices and IC's, pp.27-30,2000.

[4.20] R.Pérez, N.Mestres, X.Jordà, P.Godignon, and J.Pascual, "*Optimization of junction termination extension for the development of a 2000V planar 4H-SiC diode*", Diamond and Related Materials, vol.12, pp.1231-1235, 2000.

[4.21] R.Singh, K.G.Irvine, J.T.Richmond, and J.W.Palmour, "*High-temperature performance of 10 kilovolts 200 amperes (pulsed) 4H-SiC PiN rectifiers*", Material Science Forum, vols.389-393, pp.1265-1268, 2000.

[5.1] D. M. Caughey and R. E. Thomas, "*Carrier Mobilities in Silicon Empirically Related to Doping and Field*", Proc. IEEE, Vol. 55, pp. 2192-2193, 1967.

[5.2] I. A. Khan and J. A. Cooper, Jr., "*Measurement of High-Field Electron Transport in Silicon Carbide*", IEEE Trans. Electron Devices, vol. 47, no. 2, pp. 269-273, 2000.

[5.3] I.A.Khan and J.A.Cooper, Jr., "*Measurement of High Field Electron Transport in Silicon Carbide*", Materials Science Forum, vol. 264-268, pp. 509-512, 1998.

[5.4] Y.Sugawara, D.Takayama, K.Asano, R.Singh, J.Palmour and T.Hayashi, "*12-19kV 4H-SiC pin Diodes with Low Power Loss*", Proceedings of 2001 ISPSD, Osaka, pp.27-30, 2001.

[5.5] H.Sugimoto, S.Kinouchi, Y.Tarui, M.Imaizumi, K.Ohtsuka, T.Takami and T.Ozeki, "*Planar p-n Diodes Fabricated by MeV Energy and High Temperature Selective Implantation of Aluminum to 4H-SiC*", in Mat. Sci. Forum, vols. 353-356, pp.731-734, 2001.

END OF THESIS